Spectrochimica Acta Part A: Molecular and Biomolecular Spectroscopy 97 (2012) 892–908

Contents lists available at SciVerse ScienceDirect

Spectrochimica Acta Part A: Molecular and Biomolecular Spectroscopy

journal homepage: www.elsevier.com/locate/saa

# Molecular structure investigation and spectroscopic studies on 2,3-difluorophenylboronic acid: A combined experimental and theoretical analysis

Mehmet Karabacak [a], Etem Kose [b], Ahmet Atac [b], M. Ali Cipiloglu [b], Mustafa Kurt [c,*]

[a] Department of Physics, Afyon Kocatepe University, Afyonkarahisar, Turkey
[b] Department of Physics, Celal Bayar University, Manisa, Turkey
[c] Department of Physics, Ahi Evran University, Kirsehir, Turkey

## HIGHLIGHTS

- Molecular conformers of 2,3-difluorophenylboronic acid were investigated.
- Spectroscopic properties of 2,3-DFPBA were examined.
- The complete assignments are performed on the basis of the total energy distribution (TED).
- TDOS, PDOS and OPDOS were investigated.

## GRAPHICAL ABSTRACT

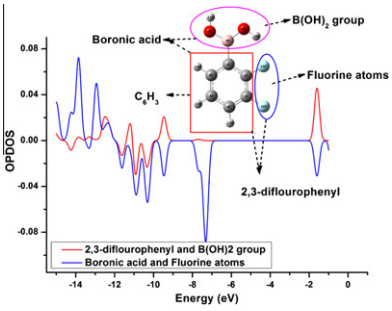


## ARTICLE INFO

*Article history:*
Received 18 May 2012
Received in revised form 6 July 2012
Accepted 22 July 2012
Available online 31 July 2012

*Keywords:*
2,3-Difluorophenylboronic acid
DFT
UV
NMR
Infrared and Raman spectra
HOMO–LUMO

## ABSTRACT

This work presents the characterization of 2,3-difluorophenylboronic acid (abbreviated as 2,3-DFPBA, $C_6H_3B(OH)_2F_2$) by quantum chemical calculations and spectral techniques. The spectroscopic properties were investigated by FT-IR, FT-Raman UV–Vis, $^1H$ and $^{13}C$ nuclear magnetic resonance (NMR) techniques. The FT-IR spectrum (4000–400 $cm^{-1}$) and the FT-Raman spectrum (3500–10 $cm^{-1}$) in the solid phase were recorded for 2,3-DFPBA. The $^1H$ and $^{13}C$ NMR spectra were recorded in DMSO solution. The UV–Vis absorption spectra of the 2,3-DFPBA that dissolved in water and ethanol were recorded in the range of 200–400 nm. There are four possible conformers for this molecule. The computational results diagnose the most stable conformer of the 2,3-DFPBA as the *trans–cis* form. The structural and spectroscopic data of the molecule were obtained for all four conformers from DFT (B3LYP) with 6-311++G (d,p) basis set calculations. The theoretical wavenumbers were scaled and compared with experimental FT-IR and FT-Raman spectra. The complete assignments were performed on the basis of the experimental results and total energy distribution (TED) of the vibrational modes, calculated with scaled quantum mechanics (SQM) method, interpreted in terms of fundamental modes. We obtained good consistency between experimental and theoretical spectra. $^{13}C$ and $^1H$ NMR chemical shifts of the molecule were calculated by using the gauge-invariant atomic orbital (GIAO) method. The electronic properties, such as excitation energies, absorption wavelengths, HOMO and LUMO energies, were performed by time-dependent DFT (TD-DFT) approach. Finally the calculation results were analyzed to simulate infrared, Raman, NMR and UV spectra of the 2,3-DFPBA which show good agreement with observed spectra.

© 2012 Elsevier B.V. All rights reserved.

* Corresponding author. Tel.: +90 386 211 45 54; fax: +90 386 252 80 54.
*E-mail addresses:* kurt@gazi.edu.tr, mkurt@ahievran.edu.tr (M. Kurt).

1386-1425/$ - see front matter © 2012 Elsevier B.V. All rights reserved.
http://dx.doi.org/10.1016/j.saa.2012.07.077

## Introduction

Interest in compounds containing boronic acid and its derivates functionality is increasing rapidly. The boronic acid (BA) and a wide variety of its derivatives are very important in various fields; such as material science, supramolecular chemistry, analytical chemistry, medicine, biology, catalysis, organic synthesis and crystal engineering. Boron-based compounds show preferential localization in tumor containing tissues making the boron-10 neutron capture therapy possible [1]. The BA analogs have been synthesized as transition state analogs for acyl transfer reactions [2] and inhibitors of dihydrotase [3]. The BA has also been incorporated into amino acids and nucleosides as anti-tumor, antiviral agents [4]. BA derivatives of divergent biologically important compounds have been synthesized as anti-metabolites for a possible two-pronged attack on cancer [5–7]. The biological application of particular dichlorophenylboronic acids was studied by Stabile et al. [8], Westmark and Smith [9].

The phenylboronic acid and its derivatives were investigated by several authors. The molecular structures of phenylboronic acid and its dimer were investigated experimentally using spectroscopic methods by Cyrański et al. [10]. Molecular structure of phenylboronic acid was investigated by Rettig and Trotte [11]. Crystal structure of pentafluorophenylboronic acid molecule was investigated by Horton et al. [12]. Shimpi et al. [13] determined crystal structures of 4-chloro- and 4-bromophenylboronic acids and hydrates of 2- and 4-iodophenylboronic acid in two different forms by single-crystal X-ray diffraction technique. The crystal structures of 3-fluorophenylboronic acid, (2,6-difluorophenyl)dihydroxyborane and 2,4-difluorophenylboronic acid were determined by Wu et al. [14], Bradley et al. [15] and Cuamatzi et al. [16], respectively. And also the crystal structure of 3-aminophenylboronic acid monohydrate and 3-formylphenylboronic acid were reported [17,18].

Infrared spectra of phenylboronic acid and diphenyl phenylboronate were studied by Faniran [19]. Theoretical and experimental analysis (DFT, FT-Raman, FT-IR and NMR) of 2-fluorophenylboronic acid were reported by Erdogdu et al. [20]. Kurt [21] investigated molecular structure and vibrational spectra of the pentafluorophenylboronic by DFT and ab initio Hartree–Fock calculations. Molecular structure, vibrational spectroscopic studies and NBO analysis of the 3,4- and 3,5-dichlorophenylboronic acid were investigated by help of the density functional method [22,23]. The experimental and theoretical vibrational spectra of 4-chloro- and 4-bromophenylboronic acids were studied by Kurt [24]. The possible stable forms and molecular structures of 2,4-dimethoxy phenylboronic acid [25] and 2,6-dimethoxy phenylboronic acid [26] were experimentally and theoretically studied using FT-IR, Raman, NMR and XRD spectroscopic methods. 2-Amino-carbonyl-phenylboronic acid and its corresponding ester, ethanediol (2-aminocarbonyl) phenylboronate were investigated computationally using both density functional theory and second-order Møller–Plesset perturbation theory [27]. Kurt et al. [28] presented an experimental and theoretical study of molecular structure and vibrational spectra of 3- and 4-pyridineboronic acid molecules by applying density functional theory calculations. *n*-butylboronic acid and methyl boronic acid were investigated by using experimental and theoretical approaches [29,30].

DFT calculations are reported to provide excellent vibrational frequencies of organic compounds if the calculated frequencies are scaled to compensate for the approximate treatment of electron correlation, for basis set deficiencies and for the anharmonicity [31–35]. Literature survey reveals that to the best of our knowledge, no experimental and computational (DFT) spectroscopic study was performed on the conformation, vibrational IR and Raman, NMR and UV–Vis spectra of the 2,3-DFPBA. In this case, the aim of this study is the detailed description of the 2,3-DFPBA molecule by using both computational and experimental techniques (FT-IR and FT-Raman, $^{13}C$ and $^{1}H$ NMR and UV–Vis spectra). For computations, we have utilized the gradient corrected DFT [36] with the Becke's three-parameter hybrid functional (B3) [37] for the exchange part and the Lee–Yang–Parr (LYP) correlation function [38], known as a cost-effective approach, for the computation of molecular structure, vibrational frequencies and energies of optimized structures.

In this study, we set out experimental and theoretical investigation of the conformation, vibrational and electronic transitions of 2,3-DFPBA. In the ground state theoretical geometrical parameters, IR, Raman, NMR and UV spectra, HOMO and LUMO energies, thermodynamic and nonlinear optical properties of title molecule were calculated by using Gaussian 09 suite of quantum chemical codes [39], for the first time. Detailed interpretations of the vibrational spectra of the 2,3-DFPBA have been made on the basis of the calculated total energy distribution (TED). The experimental results (IR, Raman, NMR and UV spectra) were supported by the computed results, comparing with experimental characterization data; vibrational wavenumbers, absorption wavelengths and chemical shifts value are in fairly good agreement with the experimental results.

## Experimental

The compound 2,3-DFPBA in solid state was purchased from Across Organics Company with a stated purity of 99% and it was used as such without further purification. The sample was prepared using a KBr disc technique. The infrared spectrum of the compound was recorded between 4000 and 400 $cm^{-1}$ on a Perkin–Elmer FT-IR system spectrum BX spectrometer. The spectrum was recorded at room temperature, with a scanning speed of 10 $cm^{-1}$ $min^{-1}$ and the spectral resolution of 4.0 $cm^{-1}$. FT-Raman spectrum of the compound was recorded between 3500 and 10 $cm^{-1}$ on a Bruker RFS 100/S FT-Raman instrument by using 1064 nm excitation from an Nd: YAG laser. The detector is a liquid nitrogen cooled Ge detector. Five hundred scans were accumulated at 4 $cm^{-1}$ resolution by using a laser power of 100 mW. The ultraviolet absorption spectra of sample solved in water and ethanol were examined in the range 200–400 nm by using Shimadzu UV-2101 PC, UV–Vis recording spectrometer. NMR experiments were performed in Varian Infinity Plus spectrometer at 300 K. The compound was dissolved in DMSO. Chemical shifts were reported in ppm relative to tetramethylsilane (TMS) for $^{1}H$ and $^{13}C$ NMR spectra. NMR spectra were obtained at the base frequency of 75 MHz for $^{13}C$ and 400 MHz for $^{1}H$ nuclei.

## Computational details

In order to obtain stable structures, the geometrical parameters including for four forms *trans–cis* (TC), *cis–cis* (CC), *cis–trans* (CT), and *trans–trans* (TT) of the 2,3-DFPBA in the ground state were optimized by using the hybrid B3LYP level of theory in DFT with the 6-311++G(d,p) basis set [37,38]. All calculations were performed by using Gaussian 09 [39]. The optimized structural parameters were used in the vibrational frequency, isotropic chemical shift and calculations of electronic properties. The vibrational frequencies, infrared and Raman intensities for the planar ($C_S$) and non-planar ($C_1$) structure of all conformers of the title molecule were calculated. Computed harmonic frequencies were scaled in order to improve the agreement with the experimental results. In our study, we have followed two different scaling factors 0.983 up to 1700 $cm^{-1}$ and 0.958 for greater than 1700 $cm^{-1}$ [40]. The total energy distribution (TED) was calculated by using the scaled quantum mechanics (SQM) method and PQS program [41,42] and the fundamental vibrational modes were characterized by their

TED. The isotropic chemical shifts are frequently used as an aid in identification of organic compounds and accurate predictions of molecular geometries are essential for reliable studies of magnetic properties. The B3LYP method allows calculating the shielding constants with accuracy and the GIAO method is one of the most common approaches for calculating nuclear magnetic shielding tensors. The $^{13}C$ and $^{1}H$ NMR isotropic shielding were calculated with the GIAO method [43] using the optimized parameters obtained from B3LYP/6-311++G(d,p) method. UV–Vis spectra, electronic transitions, vertical excitation energies, absorbance and oscillator strengths were computed with the time-dependent DFT (TD-DFT) method. The electronic properties such as HOMO and LUMO energies were determined by TD-DFT approach.

To calculate group contributions to the molecular orbitals and to prepare total density of states (TDOS or DOS) the partial density of states (PDOS) and overlap population density of states (OPDOS) spectra GaussSum 2.2 [44] was used. The contribution of a group to a molecular orbital was calculated by using Mulliken population analysis. The PDOS and OPDOS spectra were created by convoluting the molecular orbital information with Gaussian curves of unit height and a FWHM (Full Width at Half Maximum) of 0.3 eV.

## Results and discussion

The molecule of the 2,3-DFPBA, has three substituents such that $B(OH)_2$ group and two F (fluorine) atoms (at *meta*- and *ortho*- positions) attached to the planar benzene ring. All forms of the molecule are in the same plane. When model system boronic acid and two fluorine atoms were chosen to investigate the possible conformers of the 2,3-DFPBA molecule. There are four possible conformers (TC, CC, CT, TT) for the 2,3-DFPBA, illustrated in Fig. 1, depend on the positions of the hydrogen atoms bonded to oxygen, whether they are directed away from or toward the ring. The energies of different conformation of the title molecule were optimized by B3LYP/6-311++G(d,p) level of calculations. Our calculations show that *TC* form is more stable than the other conformers. Four conformers of the 2,3-DFPBA molecule energies and energy difference [the relative energy of the other conformers was as: $\Delta E = E(C_n) - E(TC)$, the conformer *TC* is the lowest energy as reference point] are determined in Table 1. According to the DFT calculation of conformers with 6-311++G(d,p) basis set, the conformer *TC* was predicted more stable from 4.8284 to 6.3162 kcal/mol (for $C_S$ symmetry group) and from 4.7605 to 6.3213 kcal/mol (for $C_1$ symmetry group) than the other conformers. We also calculated imaginary frequencies ($-52$ and $-59$ $cm^{-1}$ for CC and CT conformers, respectively) in $C_S$ symmetry group. Because of the imaginary frequency, the calculations showed that the conformers CC and CT are unstable conformers in $C_S$ point group symmetry. However, in $C_1$ point group symmetry, all conformers are stable (see Table 1). Intra-hydrogen bonds can be responsible for the geometry and the stability of a predominant conformation; the formation of hydrogen bonding between a hydroxyl and O=COH groups cause the structure of the conformer TC to be most stable conformer for 2,3-DFPBA. The stability order conformers is *trans–cis* > *cis–cis* > *cis–trans* > *trans–trans* form for 2,3-DFPBA. Therefore, in the present work we have focused on this *trans–cis* form of 2,3-DFPBA molecule. In this paper geometric parameters (bond lengths and bond angles), vibrational frequencies, NMR chemical shifts, UV absorption (electronic structure), nonlinear optical and thermodynamic features, Mulliken atomic charge of title molecule were reported by using 6-311++G(d,p) with the comparing experimental results.

### *Geometrical structures*

The geometry of the molecule under investigation is considered by possessing $C_s$ point group symmetry. The crystal structure of the 2,3-DFPBA are not available in the literature till now. Therefore, the geometric parameters, bond lengths and bond angles were

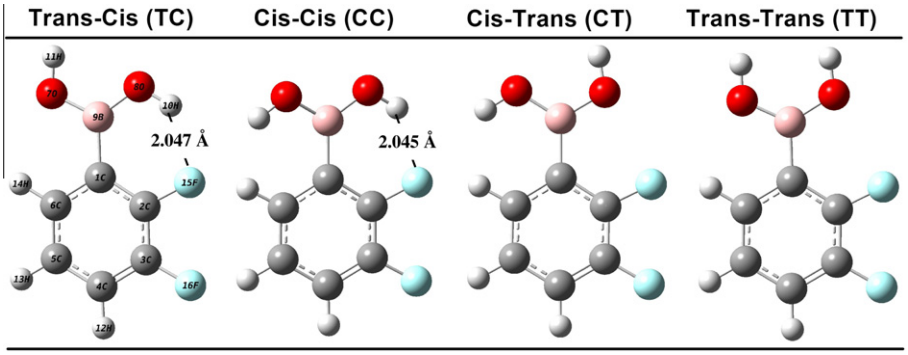


**Fig. 1.** The theoretical geometric conformers of the 2,3-DFPBA.

**Table 1**
Calculated energies and energy differences for four possible conformers (TC, CC, CT and TT) of the 2,3-DFPBA by DFT (B3LYP 6-311++ G(d,p)) method.

| Conformers | Energy | | Energy differences[a] | | Dipole moment | Imaginary frequencies |
|---|---|---|---|---|---|---|
| $C_S$ group symmetry | (Hartree) | (kcal/mol) | (Hartree) | (kcal/mol) | (Debye) | |
| *Trans–cis* | −606.93076996 | −380854.8240 | 0.0000 | 0.0000 | 1.6163 | – |
| *Cis–cis* | −606.92307536 | −380849.9956 | 0.0077 | 4.8284 | 4.2323 | 1 ($-52$ $cm^{-1}$) |
| *Cis–trans* | −606.92239190 | −380849.5667 | 0.0084 | 5.2573 | 3.9900 | 1 ($-59$ $cm^{-1}$) |
| *Trans–trans* | −606.92070450 | −380848.5078 | 0.0100 | 6.3162 | 3.9571 | – |
| $C_1$ group symmetry | | | | | | |
| *Trans–cis* | −606.93074912 | −380854.8109 | 0.0000 | 0.0000 | 1.6267 | – |
| *Cis–cis* | −606.92316278 | −380850.0504 | 0.0076 | 4.7605 | 4.1660 | – |
| *Cis–trans* | −606.92223320 | −380849.4671 | 0.0085 | 5.3438 | 3.7693 | – |
| *Trans–trans* | −606.92067554 | −380848.4896 | 0.0100 | 6.3213 | 3.9613 | – |

[a] Energies of the other three conformers relative to the most stable *Trans–Cis* conformer.

compared with the structurally similar phenylboronic acid and 2,4-difluorophenylboronic acid [11,16]. The atomic numbering schemes of all conformers (TC, CC, CT, TT) of the 2,3-DFPBA are shown in Fig. 1. The optimized geometry parameters of all conformers are given Supplementary Table S1. The optimized geometry parameters (bond lengths and bond angles) of TC conformer of the molecule are given in Table 2, comparing to the experimental values, in accordance with the atom numbering Fig. 1. From the data shown in Table 2, it is seen that the B3LYP levels of theory in general slightly underestimates some bond lengths and overestimates few bond lengths, bond angles from X-ray data. Taking into account that the molecular geometry in the vapor phase may be different from in the solid phase, owing to extended hydrogen bonding and stacking interactions there is reasonable agreement between the calculated and experimental geometric parameters.

The C–H bonds for the title molecule are approximately equal to the experimental values both of phenylboronic acid and 2,4-difluorophenylboronic acid [11,16]. The similar behaviors are valid between the C–C ring bond lengths and angles. For example, the optimized bond lengths of the C–C bond in ring systems were calculated in the range of 1.387–1.410 Å for 2-fluorophenylboronic acid [20] and observed at 1.365 and 1.406 Å for 3-flurophenylboronic acid [14], also from 1.378 to 1.404 Å in the phenylboronic acid (=pba), and from 1.363 to 1.394 Å in 2,4-difluorophenylboronic acid [11,16]. In this study, we calculated the CC bond lengths in the ranges 1.384–1.395 Å that show well coherent with above studies.

Generally, typical B–O distances are ca. 1.360 Å [12] consistent with relatively strong π-interactions. Conversely, the B9–O7 bond length is slightly greater than that typically found in boroxines, indicating a weakening of this bond by the electron-withdrawing nature of the ring part. However, Chen et al. [4] found approximately the same value of this bond length by using HF/6-31G(d) levels of theory, for the few boronic acids including phenylboronic acid molecule. For the 3,5-dichlorophenylboronic acid, this bond length for different forms were found in the range of 1.364–1.372 Å [22], and also in the previous work, B–O distances including for different forms were calculated from 1.366 to 1.373 Å ranges for 3,4-dichlorophenylboronic acid [23]. For the 2,4- and 2,6-dimethoxyphenylboronic acid molecule B–O distances including CT ($C_S$) and CT ($C_1$) forms were found from 1.371 to 1.375 Å and other forms were found from 1.365 to 1.373 Å [25,26]. For our title molecule, the optimized B–O bond lengths were obtained in the range 1.359–1.374 Å.

The O–H bonds for the title molecule are about equal to the experimental values. These bond lengths were calculated at 0.963 Å for O7–H11 and O8–H10. Experimental values of O–H bonds of phenylboronic acid and 2,4-difluorophenylboronic acid are 0.750 and 0.841 Å, respectively.

The optimized B–C bond lengths were calculated at 1.575 Å for the 2,3-DFPBA. The experimental values of phenylboronic acid and 2,4-difluorophenylboronic acid are in well coherent, observed 1.568 and 1.566 Å [11,16]. Bhat et al. [27] calculated B–C bond lengths at 1.566 and 1.567 Å in the most stable form for phenylboronic acid by using B3LYP and MP2 methods, respectively. The $C_6$–$B_{12}$ bond length is slightly larger than that typically found in boroxines, indicating a weakening of this bond by the electron-withdrawing nature of the $C_6$ $F_5$ group [21]. This calculated bond lengths show very good correlation with structurally similar molecules [20–26].

The C–X (X; F, Cl, Br . . .) bond length indicates a considerable increase when substituted in place of C–H. This band (fluorine atom) were calculated at 1.318–1.356 for 2,3-difluoro phenol molecule [45] and observed good correlation for 2,6-difluoro phenol molecule [46]. The bond distance C–F is approximately similar at 1.357 Å [47] which is in good agreement with calculated value in the previous study for 5-fluoro-salicylic acid [48]. Horton et al. the $C_{12}$–$F_{15}$ and $C_{13}$–$F_{16}$ observed 1.349 and 1.342 Å in pentafluorophenylboronic acid [12], and Kurt [21] calculated these bonds 1.357 and 1.336 Å using B3LYP/6-311G(d,p) basis sets. In this paper we obtained at 1.362 and 1.347 Å ($C_2$–$F_{15}$ and $C_3$–$F_{16}$) respectively. These bonds also show good agreement with observed values of 2,4-difluorophenylboronic acid [16].

The ring C–C–C bond angles were calculated at 116.4–122.4° which is good correlation with the experimental values and normal values (120.0°) of the six-membered phenyl ring. However the C2–C1–C6 bond angle deviated from normal value, this may be due to the attached $B(OH)_2$ group.

Two hydrogen atoms are in the O–B–O plane. Most probably, the oxygen lone pairs have a resonance interaction with the empty *p* orbital of boron, which forces the hydrogen to be in the O–B–O plane. From the calculations, the optimized structure of 2,3-DFPBA was calculated to exist in a planar structure for the TC and TT forms, while the other forms of the molecule were calculated to exist as a nearly planar structure with C–C–B–O torsional angle (ca. 13° the CC form, 34° for CT form by using 6-311++G(d,p) basis set).

All the geometrical parameters were simultaneously relaxed during the calculations while the C–C–B–O torsional angle was varied in steps of 10°. The resulted potential energy curve depicted in Supplementary Fig. S1 shows TC form for minimum energies. The

**Table 2**
Bond lengths (Å) and bond angles (°) experimental and optimized of the 2,3-DFPBA for *Trans–cis* conformer.

| Parameters bond lengths (Å) | X-ray [a, b] | | B3LYP6-311++G(d,p) |
|---|---|---|---|
| C1–C2 | 1.404 (3) | 1.382 (3) | 1.392 |
| C1–C6 | 1.402 (3) | 1.394 (3) | 1.407 |
| B9–C1 | 1.568 (3) | 1.566 (3) | 1.575 |
| C2–C3 | 1.389 (3) | 1.370 (3) | 1.389 |
| C2–F15 | – | 1.364 (3) | 1.362 |
| C3–C4 | 1.378 (5) | 1.363 (4) | 1.384 |
| C3–F16 | – | 1.358 (3) | 1.347 |
| C4–C5 | 1.384 (5) | 1.366 (4) | 1.395 |
| C4–H12 | 1.000 (5) | – | 1.083 |
| C5–C6 | 1.390 (4) | 1.374 (3) | 1.391 |
| C5–H13 | 1.000 (5) | 0.930 | 1.083 |
| C6–H14 | 1.000 (5) | 0.930 | 1.083 |
| B9–O7 | 1.378 (2) | 1.338 (3) | 1.366 |
| O7–H11 | 0.750 (5) | 0.841 (15) | 0.963 |
| B9–O8 | 1.362 (2) | 1.361 (3) | 1.366 |
| O8–H10 | 0.750 (5) | 0.841 (15) | 0.963 |
| H10–F15 | | | 2.055 |
| Bond Angles (°) | | | |
| C2–C1–C6 | 117.2 (2) | 114.6 (2) | 116.4 |
| C2–C1–B9 | 120.8 (2) | 125.3 (2) | 123.2 |
| C6–C1–B9 | 122.0 (2) | 120.1 (2) | 120.3 |
| C1–C2–C3 | 121.8 (2) | 125.1 (2) | 122.4 |
| C1–C2–F15 | – | 118.2 (2) | 120.2 |
| C3–C2–F15 | – | 116.7 (2) | 117.3 |
| C2–C3–C4 | 119.5 (3) | 116.4 (2) | 120.3 |
| C2–C3–F16 | – | 118.1 (2) | 119.4 |
| C4–C3–F16 | – | 118.8 (2) | 120.4 |
| C3–C4–C5 | 120.3 (2) | 123.0 (2) | 118.9 |
| C3–C4–H12 | 120.0 (2) | – | 119.0 |
| C5–C4–H12 | 120.0 (2) | – | 122.1 |
| C4–C5–C6 | 120.1 (3) | 117.9 (2) | 120.3 |
| C4–C5–H13 | 120.0 (2) | 121.0 | 119.5 |
| C6–C5–H13 | 120.0 (2) | 121.0 | 120.2 |
| C1–C6–C5 | 121.1 (2) | 122.9 (2) | 121.7 |
| C1–C6–H14 | 120.0 (2) | 118.5 | 118.2 |
| C5–C6–H14 | 120.0 (2) | 118.5 | 120.1 |
| B9–O7–H11 | 111.0 (1) | 116 (2) | 112.3 |
| B9–O8–H10 | 111.0 (1) | 115 (2) | 114.2 |
| C1–B9–O7 | 118.7 (2) | 117.4 (2) | 117.1 |
| C1–B9–O8 | 125.0 (2) | 123.8 (2) | 124.7 |
| O7–B9–O8 | 116.3 (2) | 118.7 (2) | 118.2 |

[a,b] The X-ray data from Ref. [11,16].

B–C rotational barrier in TT and CC form was calculated to be ca. 4–6 kcal/mol (Supplementary Fig. S1), which is significantly high as compared the B–C barrier TC form of molecule.

*Vibrational spectral analysis*

The present molecule which has $C_S$ symmetry consist of 16 atoms, so it has 42 fundamental vibrational modes. These modes are represented by symmetry species 29A' + 13A'', with the *A*' representing in-plane motions and *A*'' representing out-of plane motions. All vibrations are active in both IR and Raman. In this form $B(OH)_2$ group and benzene ring are in the same plane. The CC and CT forms of molecule are non-planar structure and have C1 symmetry and the vibrational modes span the irreducible representations: 42A. The experimental wavenumbers are tabulated in Table 3 together with the calculated wavenumbers for the most stable conformer (TC) of studied molecule. The symmetry species of all the vibrations are given in the second column and in the last column is given a detailed description of the normal modes based on the total energy distribution (TED).

In order to obtain the spectroscopic signature of the 2,3-DFPBA, we performed a wavenumber calculation analysis by using DFT/B3LYP/6-311G++(d,p) basis set [39]. The calculations were made for free molecule in gas phase, while experiments were performed for solid sample, therefore there are disagreements between calculated and observed vibrational wavenumbers, and some frequencies are calculated, however these frequencies are not observed in the FT-IR and FT-Raman spectra. To the best of our knowledge there is no vibrational data for gas phase of the title molecule. Therefore we compared calculated results with those of solid phase of vibrational spectrum of title molecules. The experimental and calculated infrared and Raman spectra were given in Fig. 2. The calculated IR and Raman spectra are shown in figure for comparative purpose, where the calculated intensity is plotted against harmonic vibrational wavenumbers.

The goal of this part of the study is the assignment of the vibrational wavenumbers. As seen in Table 3, there is great mixing of the ring vibrational modes and also between the ring and substituent modes. The descriptions of the modes are very complex because of the low symmetry of the studied molecule. Especially,

**Table 3**
Comparison of the calculated harmonic frequencies and experimental (FT-IR and FT-Raman) wavenumbers ($cm^{-1}$) using by B3LYP method 6-311++G(d,p) basis set for *Trans–cis* conformer of 2,3-DFPBA.

| Modes no | Sym. species | Theoretical | | Experimental | | TED [b] (⩾10%) |
|---|---|---|---|---|---|---|
| | | Unscaled freq. | Scaled freq.[a] | FT-IR | FT-Raman | |
| ν1 | *A*′ | 3854 | 3692 | 3400 | | νOH (100) ($O_8$–$H_{10}$) |
| ν2 | *A*′ | 3847 | 3685 | 3332 | | νOH (100) ($O_7$–$H_{11}$) |
| ν3 | *A*′ | 3204 | 3070 | 3070 | 3075 | νCH (100) |
| ν4 | *A*′ | 3199 | 3064 | | 3055 | νCH (100) |
| ν5 | *A*′ | 3182 | 3048 | | 3040 | νCH (100) |
| ν6 | *A*′ | 1657 | 1629 | 1628 | 1626 | νCC (71) |
| ν7 | *A*′ | 1618 | 1590 | 1588 | 1590 | νCC (67) + δCCH (12) |
| ν8 | *A*′ | 1503 | 1478 | 1475 | 1474 | δCCH (42) + νCC (33) |
| ν9 | *A*′ | 1491 | 1465 | 1468 | | νCC (39) + δCCH (28) |
| ν10 | *A*′ | 1394 | 1371 | | 1389 | νβ$O_2$ asym. (80) |
| ν11 | *A*′ | 1369 | 1345 | 1352 | 1351 | νβ$O_2$ sym. (33) + νCB (25) + δβOH (18) |
| ν12 | *A*′ | 1327 | 1304 | | 1292 | νCC (88) |
| ν13 | *A*′ | 1286 | 1264 | 1266 | 1269 | δCCH (37) + νCF (33) + νCC (20) |
| ν14 | *A*′ | 1234 | 1213 | 1214 | 1215 | δCCH (44) + νCC (28) + νCF (11) |
| ν15 | *A*′ | 1190 | 1170 | 1183 | 1178 | νCF (39) + δCCH (20) + δCCC (15) |
| ν16 | *A*′ | 1169 | 1149 | 1154, 1134 | 1148 | νCC (45) + δCCH (23) |
| ν17 | A' | 1081 | 1063 | 1062 | 1065 | νCC (51) + δCCH (31) |
| ν18 | *A*′ | 1044 | 1026 | 1040 | 1030 | δβOH (95) i.p OH bending |
| ν19 | *A*′ | 1020 | 1002 | | | δβOH (60) i.p OH bending + νBO (33) |
| ν20 | *A*″ | 984 | 968 | 978 | | γCH (92) |
| ν21 | *A*″ | 928 | 912 | 907 | 911 | γCH (90) |
| ν22 | A' | 915 | 899 | | | νCF (27) + δCCC (25) + νBO (17) + νCB (12) |
| ν23 | *A*′ | 828 | 814 | 818 | 822 | δCCC (33) + νCF (26) + δCCH (18) + νCC (14) |
| ν24 | *A*″ | 806 | 792 | 792 | 804 | γCH (81) |
| ν25 | *A*″ | 742 | 729 | 731 | | γCH [τCCCC(22) + τCCCH(22)] + τCCBO (19) |
| ν26 | *A*″ | 671 | 660 | 664 | 662 | τCCBO (25) + τBOOH (19) + τCBOH (13) + τCCCC (12) |
| ν27 | *A*′ | 646 | 635 | 648 | | νCC (30) + νCF (24) + νCβ (17) |
| ν28 | *A*″ | 601 | 591 | | 597 | γOH (84) |
| ν29 | *A*′ | 584 | 574 | | 580 | δCCF (48) + δCCC (28) |
| ν30 | *A*″ | 567 | 557 | 568 | 556 | τCCCC (31) + γOH (28) + τCCCH (11) |
| ν31 | *A*″ | 534 | 524 | | | γOH (65) + τCCCC (14) |
| ν32 | *A*′ | 522 | 513 | 502 | 501 | δOBO (34) + δCBO (16) + δCCC (12) |
| ν33 | *A*′ | 484 | 475 | | 465 | δCCC (42) + δCCF (29) + νCF (12) |
| ν34 | *A*″ | 467 | 459 | 460 | | τCCCC (28) + τCBOH (21) + τCCCF (20) + τCCBO (13) |
| ν35 | *A*′ | 360 | 353 | | 350 | δCBO (69) + δCCF (14) |
| ν36 | *A*′ | 318 | 312 | | 310 | δCBO (36) + νCB (26) + δCCF (25) |
| ν37 | *A*′ | 304 | 299 | | | δCCF (72) + δCCB (12) |
| ν38 | *A*″ | 296 | 291 | | | τCCCF (64) + τCCCC (13) |
| ν39 | *A*″ | 208 | 204 | | 228 | τCCCF (33) + τCFCF (17) + τCCCC (15) + τCCCB (15) |
| ν40 | *A*′ | 168 | 165 | | | Rocking ($BO_2H_2$[δCCB (68) + δCBO (22)] |
| ν41 | *A*″ | 100 | 99 | | 100 | τCCCB (38) + τFCCB (18) + τCCCC (13) + τCCBO (13) |
| ν42 | *A*″ | 59 | 58 | | | τCCB$O_8$ (50) + τCCB$O_7$ (48) |

[a] Wavenumbers in the ranges from 4000 to 1700 $cm^{-1}$ and lower than 1700 $cm^{-1}$ are scaled with 0.958 and 0.983 for B3LYP/6-311++G(d,p) basis set, respectively.
[b] TED: Total energy distribution ν; stretching, γ; out-of-plane bending, δ; in-plane-bending, τ; torsion.

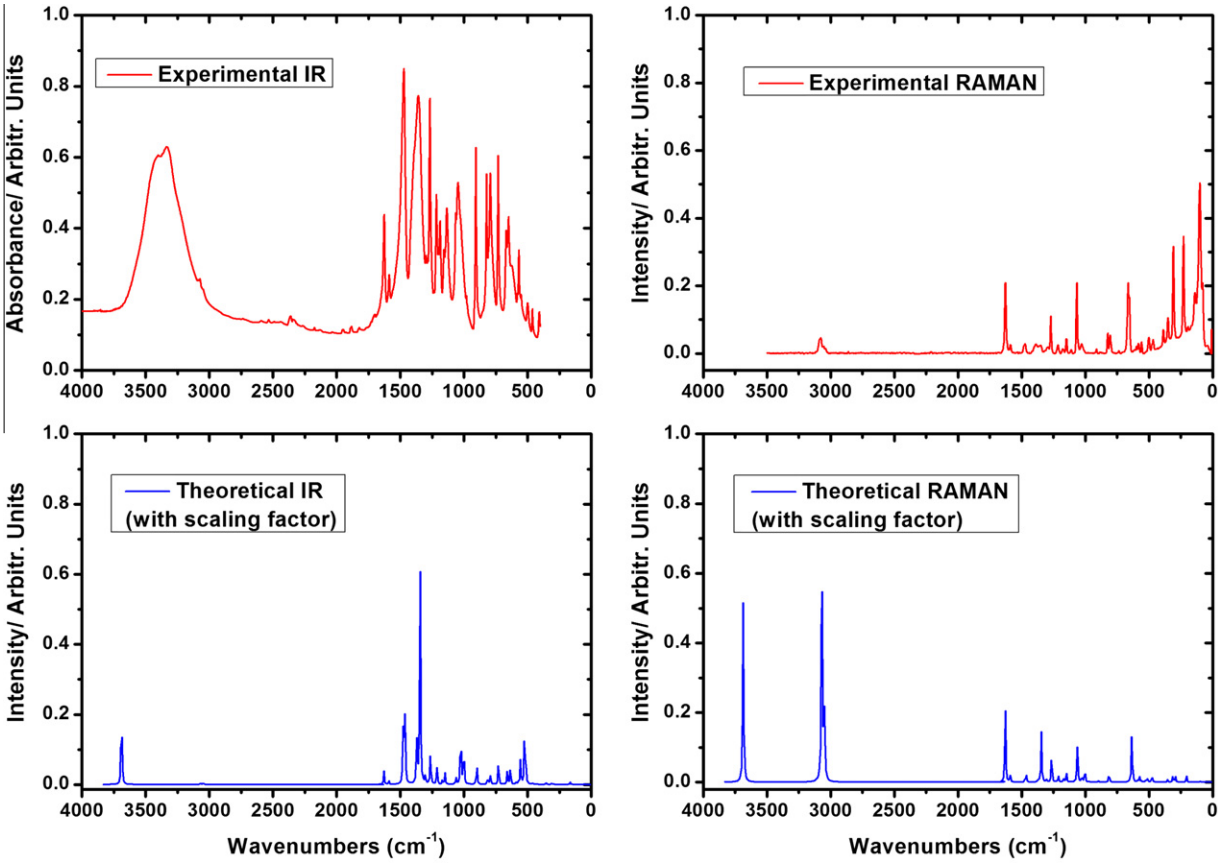


**Fig. 2.** The experimental and calculated infrared and Raman spectra of the 2,3-DFPBA.

in-plane and out-of-plane modes are the most difficult modes to be assigned due to the mixing with the ring modes and also with the substituent modes. But there are some strong frequencies useful to characterize in the IR and Raman spectrum. It is worth mentioning that, for our molecule, the stretching and bending vibrational modes are OH, CH, CC, CF, BO, CB and CCH, BOH, CCC, CCF, CBO, CCB, OBO, respectively, and also, ring bending and ring torsion modes assigned out-of plane bending of C–H and O–H are the bending vibrational modes for title molecule.

*OH modes*

The O–H vibrations are extremely sensitive to formation of hydrogen bonding. The O–H stretching band is characterized by very broad band appearing near about 3400–3600 $cm^{-1}$. In the O–H region, very strong and broad bands in the spectra of some boronic acid molecules occur at ca. 3300 $cm^{-1}$. The assignment of these bands called as O–H stretching vibrations is comprehensible. In the spectra of phenylboronic acid (3280 $cm^{-1}$ in IR) [19], 2-fluorophenylboronic acid (3467 $cm^{-1}$ in FT-IR) [20], pentafluorophenylboronic acid, (3467, 3410 $cm^{-1}$ in FT-IR) [21], 3,5 dichlorophenylboronic acid (3443, 3397 $cm^{-1}$ in FT-IR and 3480, 3440 $cm^{-1}$ in FT-Raman) [22], 3,4 dichlorophenylboronic acid (3465, 3425 $cm^{-1}$ in FT-IR) [23], 4-chloro and 4-bromophenylboronic acid (3276, 3249 and 3276, 3164 $cm^{-1}$ in FT-IR) and (3175, 3106 and 3108 $cm^{-1}$ in FT-Raman) [24], 2,4-dimethoxyphenylboronic acid (3480, 3339 $cm^{-1}$ in FT-IR) [25], 2,6-dimethoxyphenylboronic acid (3335 $cm^{-1}$ in FT-IR and 3278 $cm^{-1}$ in FT-Raman) [26] were assigned, which is typical for O–H bonded hydroxyl groups. The strength and broadening wavenumbers of these bands suggest that intramolecular hydrogen bonding occurs in different environments of boronic acids [19]. In this study, the two O–H stretching vibrations were recorded at 3332 and 3400 $cm^{-1}$ in FT-IR spectrum and predicted value of 3685 ($O_7$–$H_{11}$) and 3692 $cm^{-1}$ ($O_8$–$H_{10}$) that show agreement with recorded FT-IR spectrum. As expected, this mode is pure stretching mode as it is evident from TED column, it is almost contributing 100%. The same vibration isn't occurred in the FT-Raman. As discussed in literature, [20–24] with halogen (F, Cl, Br...) substitution, O–H stretching vibrations shift to a higher wavenumber region [49]. This means that, in the boronic acid part, O–H vibrations are sensitive due to the halogen coordination.

The modes ν18 and ν19 as a OH in-plane bending were predicted at 1026 and 1002 $cm^{-1}$ and out-of-plane bending vibrations (ν26, ν28, ν30 and ν31) were computed at 524, 557, 591 and 660 $cm^{-1}$. These bands were assigned at 1030 $cm^{-1}$ in FT-Raman and 1040 $cm^{-1}$ in FT-IR bands (in-plane) while OH out-of-plane bending vibrations were assigned at 568 and 664 in FT-IR $cm^{-1}$ and 556, 597 and 662 $cm^{-1}$ in FT-Raman, respectively. Theoretical values of OH out-of-plane bending and in-plane bending vibration are in good agreement with the experimental values and literature data [20–26].

*C–H modes*

The hetero-aromatic structure shows the presence of the C–H stretching vibration in the 3000–3100 $cm^{-1}$ range which is the characteristic region for ready identification of C–H stretching vibration [50]. In this region, the bands are not affected appreciably by the nature of the substituents. 2,3-DFPBA has two adjacent and one isolated C–H moieties. In aromatic compounds, C–H in-plane bending frequencies appear in the range of 1000–1300 $cm^{-1}$ and C–H out-of-plane bending vibration in the range 750–1000 $cm^{-1}$ [50,51]. These modes were discussed in the literature and

predicted in the range of 3048–3070 $cm^{-1}$ for structurally similar compounds [20–24]. The modes 3–5 correspond to the stretching modes of $C_4$–H, $C_5$–H and $C_6$–H units. These modes were computed at 3048, 3064 and 3070 $cm^{-1}$ by the B3LYP/6-311++G(d,p) method and observed at 3070 $cm^{-1}$ in FT-IR and recorded at 3040, 3055 and 3075 $cm^{-1}$ FT-Raman, showing good agreement. They are pure modes since their TED contribution 100%. The aromatic C–H stretching bands are found to be weak, and this is due to a decrease in the dipole moment caused by reduction of negative charge on the carbon atom.

The aromatic C–H in-plane bending vibrations lie in the region of 1230–970 $cm^{-1}$. The C–H in-plane bending vibrations were observed at 1266, 1214, 1183 $cm^{-1}$ in FT-IR and 1269, 1215, 1178 $cm^{-1}$ in FT-Raman. These modes are predicted at 1264, 1213 1170 $cm^{-1}$. The C–H out-of-plane bending modes are assigned $\nu_{25,24,21,20}$ and predicted at 729, 792, 912, 968 $cm^{-1}$, respectively. These modes were observed at 731, 792, 907, 978 and 804, 911 $cm^{-1}$ in FT-IR and FT-Raman, respectively. The TED contributions of in-plane and out-of-plane modes indicate that these vibrations are contaminated with other modes. All results for the above conclusions are in well agreement with the literature of the similar molecules [20–24].

*CC modes*

The ring stretching vibrations are very much important and highly characteristic of the aromatic ring itself. The ring carbon–carbon stretching vibrations occur in the region 1625–1430 $cm^{-1}$. In general, the bands are of variable intensity and are observed at 1625–1590, 1590–1575, 1540–1470, 1465–1430 and 1380–1280 $cm^{-1}$ from the frequency ranges given by Varsanyi [52] for the five bands in the region. For phenylboronic acids, the aromatic C–C stretching regions were assigned in the range of 1620–1320 $cm^{-1}$ in the IR spectra [19]. Similarly, the C–C stretching modes were recorded for 2-fluorophenylboronic acid in the range of 1617–1034 $cm^{-1}$ [20], 3,5-dichlorophenylboronic acid in the range of 1570–969 $cm^{-1}$ in FT-IR and 1584–995 $cm^{-1}$ in FT-Raman [22], 3,4-dichlorophenylboronic acid at 1591–1028 $cm^{-1}$ in FT-IR and 1590–1035 $cm^{-1}$ in FT-Raman [23], 4-chlorophenylboronic acid 1596–1060 and 1588–1085 $cm^{-1}$ in FT-IR and FT-Raman and 4-bromophenylboronic acid at the range of 1590–1010 and 1588–1004 $cm^{-1}$ in FT-IR and FT-Raman, respectively [24]. Also these results [20,22–24] were supported DFT calculations computed ca. 1600–990 $cm^{-1}$ using B3LYP calculations. In the present work, C–C stretching vibrations were calculated 1629–1465, 1304–1213, 1149, 1063 and 635 $cm^{-1}$ by B3LYP method for 2,3-DFPBA and observed at 1628, 1588, 1475, 1468, 1266, 1214, 1154, 1134, 1062 and 648 $cm^{-1}$ in FT-IR and 1626, 1590, 1474, 1292, 1269, 1215, 1148 and 1065 $cm^{-1}$ in FT-Raman, showed very well correlation with each other. The main C–C stretching vibrations are calculated at 1304 $cm^{-1}$ with the TED contribution 85%.

The ring deformation, torsion and CCC bending modes contaminated with other modes. The calculated wave numbers of these modes almost coincide with experimental data after scaling. The ring deformation, torsion and out-of-plane CCC bending modes are obtained in a large region. The TEDs of these vibrations are not pure modes as it is evident from the last columns of Table 3.

*C–F modes*

In the fluorine compounds, very intense absorption of CF mode occurs in the region 1100–1350 $cm^{-1}$ [49,53]. Infrared spectra of mono- and di-substituted fluorine derivatives have been studied by Narasimham et al. [54] and those of tri- and tetrafluorobenzene by Ferguson et al. [55]. They have assigned the frequency at 1250 $cm^{-1}$ to C–F stretching mode of vibration. In analogy to these assignments, infrared frequency observed at 1235 $cm^{-1}$, is assigned as C–F stretching frequency for 1-fluoro-2,4-dinitrobenzene [56], corresponding Raman frequency for the same mode is 1246 $cm^{-1}$. For 2,3-difluoro phenol, Sundaraganesan et al. [45] assigned the strong bands at 1331 and 1279 $cm^{-1}$ in FT-IR spectrum due to C–F stretching mode, and their counterpart in Raman spectrum is at 1332 and 1280 $cm^{-1}$. In previous study, we have assigned the strong bands at 1254 and 1222 $cm^{-1}$ in the FT-IR spectrum due to the C–F stretching mode. Their counterpart in the Raman spectrum is at 1274 and 1245 $cm^{-1}$. The theoretically computed scaled value of 1271 and 1240 $cm^{-1}$ at B3LYP/6-311 + G(d,p) showed good agreement with experimental results for 5-flouro salicylic acid [48]. This bands at 1004, 1001 and 996 $cm^{-1}$ were assigned as a C–F stretching vibrations for some pentafluoro-compounds [57] and pentafluoro-benzyl-bromide [58] molecule. CF stretching modes were computed at 1264–1170 and 899, 814, 635 $cm^{-1}$ showed in well correlation with the experimental values.

The C–F in-plane bending frequency appears in the region 350–250 $cm^{-1}$ [59]. The C–F in-plane bending wavenumbers were computed by B3LYP method in the region 380–255 $cm^{-1}$ for pentaflourophenyl boronic acid [21]. The band at 292 $cm^{-1}$ in FT-Raman was assigned to C–F in-plane bending mode for 2,3-difluorophenol [45]. Sundaraganesan et al. [60] observed strong band at 759 $cm^{-1}$ in FT-IR and very strong band at 750 $cm^{-1}$ in FT-Raman assigned to C–F in-plane bending mode for 2-amino-4,5-difluorobenzoic acid molecule. The C–F out-of-plane bending mode was identified as the frequency at 590 $cm^{-1}$ as a weak band in FT-IR and 592 $cm^{-1}$ in FT-Raman [60]. For 2-fluorophenylboronic acid molecule, Erdogdu et al. [20] observed one band at 520 $cm^{-1}$ both in the FT-IR and in the FT-Raman spectra. The C–F out-of-plane bending modes of the bands are supported in literature [60–63]. In our present work we predicted at 574, 475, 353, 312, 299 $cm^{-1}$ for C–F in-plane bending modes and 291 and 204 $cm^{-1}$ for C–F out-of-plane bending modes. We also identified according to TED as a major contribution mode 37 and 29 for in-plane modes. The values are supported in very good agreement with the experimental results (see Table 3).

*B–O modes*

The B–O asymmetric stretching band of the phenylboronic acid occurs at 1370 $cm^{-1}$ in the infrared spectrum [19] and at 1375 $cm^{-1}$ for the phenylboronic acid linkage [64]. These bands are very intense and should also include the asymmetric stretching vibrations which are located at 1349 and 1350 $cm^{-1}$ for phenylboronic, and pentafluorophenylboronic acids, respectively [19,21]. Vargas et al. [65] assigned the band around at 1370 $cm^{-1}$ as the ν(B–O) stretching vibrations for the homo-and hetero tri-nuclear boron complexes. For 2-fluorophenylboronic acid these bands were observed at 1385 $cm^{-1}$ in the FT-IR and 1370 $cm^{-1}$ in the FT-Raman spectra [20]. The corresponding bands were observed at 1392 $cm^{-1}$ as very strong bands in FT-IR and at 1409 $cm^{-1}$ as weak bands in FT-Raman spectra [22]. The other strong band in the spectrum observed at 1379 $cm^{-1}$ [23]. This band is very intense and should include also the ν(B–O) asymmetric stretching vibration. Kurt [24] observed the νB–O stretching vibration at 1373 and 1361 $cm^{-1}$ for 4-chlorophenylboronic acid and 4-bromophenylboronic acid, respectively. These modes also were calculated at ca. 1400–1350 $cm^{-1}$ by using B3LYP method and determined, when two chlorine or fluorine atoms are substituted on phenylboronic acid, the B–O vibration shifts to higher wavenumbers in the spectrum [20–23]. In our study for the 2,3-DFPBA derivatives of the phenyl boronic acid, νB–O stretching vibrations were observed at 1352, 1351 (symmetric stretching) and 1389 $cm^{-1}$ (asymmetric stretching). We calculated symmetric and asymmetric stretching vibrations at 1345 and 1371 $cm^{-1}$ by using B3LYP method, respectively. The TED calculations show that the B–O stretching (mode 10) is clearly a pure mode in Table 3. We can also say when two

fluorine atoms are substituted at the second and third positions phenylboronic acid, the B–O vibration shifts to higher wavenumbers of ca. 10 and 5, ca. 18 $cm^{-1}$ in the FT-IR spectrum and FT-Raman spectrum, respectively.

*C–B modes*

The C–B stretching modes were observed at 1080 and 1110 $cm^{-1}$ for vibration of the arylboronic acid by Bradley [15]. Faniran et al. [19] also assigned the band at 1089 and 1085 $cm^{-1}$ in the spectra of the normal and deuterated phenylboronic acids, respectively, and at 1084 $cm^{-1}$ in diphenyl phenylboronate to the C–B stretching modes. The C–B stretching bands were observed at 1354 $cm^{-1}$ in the infrared spectrum and were shifted by 265 $cm^{-1}$ for the fluorine substitution. This means that in the boronic acid part C–B vibrations are sensitive because of fluorine substitution [20]. For *n*-butylboronic acid, these vibrations are assigned at 1147 and 1109 $cm^{-1}$ by Cyrański et al. [29]. For 3,5-dichlorophenylboronic molecule this vibration was observed at 802 $cm^{-1}$ as medium bands in FT-IR. The C–B stretching band of this molecule was negatively shifted by ca. 280 $cm^{-1}$ for the chlorine substitution [22]. These means those in the boronic acid part C–B vibrations are sensitive because of chlorine or fluorine substitution [20,22].

*Error analysis of different vibrational calculations*

We plotted correlation graphics between the experimental and calculated wavenumbers obtained by DFT/B3LYP method. The correlation graphics which described harmony between the calculated and experimental wavenumbers (Raman and Infrared) were given in (Fig. 3a and b). As can be seen from figures, experimental fundamentals have a better correlation with B3LYP. The relations between the calculated and experimental wavenumbers are linear and described for Raman and Infrared, respectively by the following equations:

$$\upsilon_{cal} = 0.9177\ \upsilon_{exp.} + 85.055 \quad (R^2 = 0.9953 \quad \text{for infrared})$$

$$\upsilon_{cal.} = 0.9974\ \upsilon_{exp.} + 23.975 \quad (R^2 = 0.9991\ \text{for Raman})$$

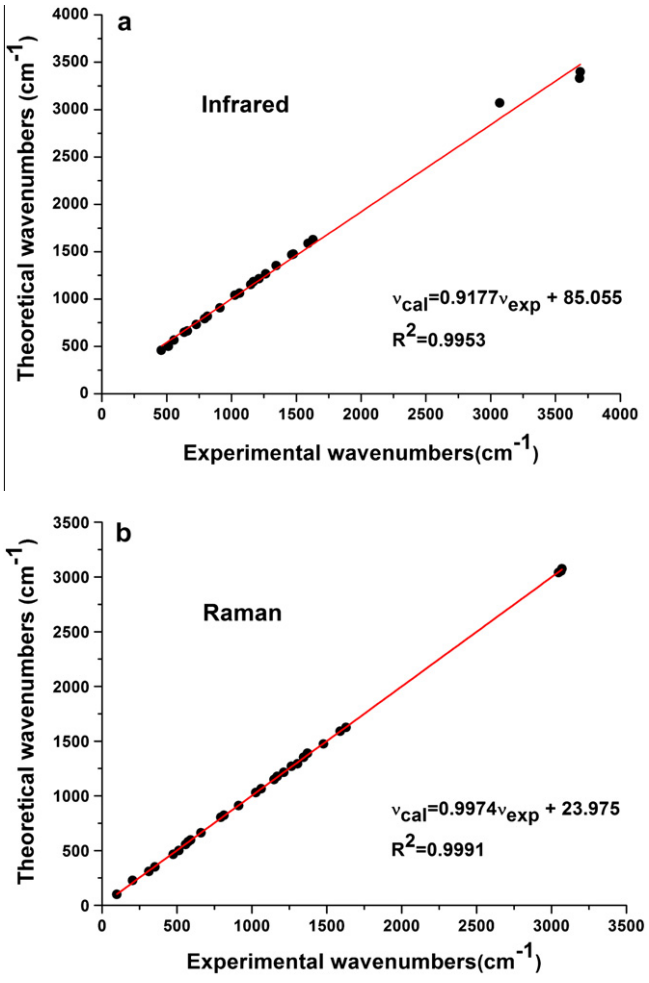


**Fig. 3.** Correlation graphics of calculated and experimental frequencies (a) Infrared (b) Raman for the 2,3-DFPBA.

*NMR spectra*

The experimental $^1H$ and $^{13}C$ NMR spectra of the 2,3-DFPBA are shown in Fig. 4a and b, respectively. The recorded and calculated $^1H$ and $^{13}C$ chemical shifts in DMSO solution solvent are collected in Table 4, the atom states were numbered according to Fig. 1.

It is recognized that accurate predictions of molecular geometries are essential for reliable calculations of magnetic properties. Firstly, full geometry optimization of the 2,3-DFPBA was performed at the gradient corrected DFT by using the hybrid B3LYP method based on Becke's three parameters functional. Then, gauge-including atomic orbital (GIAO) $^1H$ and $^{13}C$ chemical shift calculations of the compound was made by the same method by using 6-311++G(d,p) basis set IEFPCM/DMSO solution. Application of the GIAO [43] approach to molecular systems was significantly improved by an efficient application of the method to the ab initio SCF calculation, by using techniques borrowed from analytic derivative methodologies. The isotropic shielding values were used to calculate the isotropic chemical shifts $\delta$ with respect to tetramethylsilane (TMS) $\delta^x_{iso} = \sigma^{TMS}_{iso} - \sigma^x_{iso}$ The values of $\sigma^{TMS}_{iso}$ is 182.46 and 31.88 ppm for $^{13}C$ and $^1H$ NMR spectra, respectively.

Aromatic carbons give signals in overlapped areas of the spectrum with chemical shift values from 100 to 150 ppm [66,67]. In this work present molecule has six different carbon atoms, which is consistent with the structure on basis of molecular symmetry. Taking into account that the range of $^{13}C$ NMR chemical shifts C2 and C3 are observed and calculated greater than this range, this shift can be due to the fluorine atom attached to these carbons. Namely, the fluorine atoms that electronegative substituent polarizes the electron distribution in its bond to carbon, therefore, the chemical shifts value of C2 and C3 bonded to fluorine atoms show that the calculated $^{13}C$ chemical shifts is too high. The chemical shift of these carbons was observed at 154.30 and 151.01 ppm while which was calculated 164.65 and 159.38 ppm, respectively. Besides, due to the shielding effect which has the non-electronegative property of $B(OH)_2$ group, the chemical shift value of C1 atom is lower than the other carbon peaks. Moreover, DMSO contains electronegative atoms such as oxygen and sulphur. Thus, our title molecule was affected this solution. The other $^{13}C$ NMR chemical shifts in the ring for the title molecule are range in from 100 to 150 ppm both experimentally and theoretically showing good correlation with each other (Table 4).

Generally, the proton chemical shift of organic molecules varies greatly with the electronic environment of the proton. Hydrogen attached or nearby electron-withdrawing atom or group can decrease the shielding and move the resonance of attached proton towards to a higher frequency, whereas electron-donating atom or group increases the shielding and moves the resonance towards to a lower frequency [68]. The chemical shifts of aromatic protons of organic molecules are usually observed in the range of 7.00–8.00 ppm. The studied molecule has three hydrogen atoms in the ring, two hydrogen atoms attached to the oxygen atom of hydroxyl group. As can be seen from the Table 4, $^1H$ isotropic chemical shifts were calculated 7.94, 7.44, 7.32, 6.88 and 6.02 ppm, observed

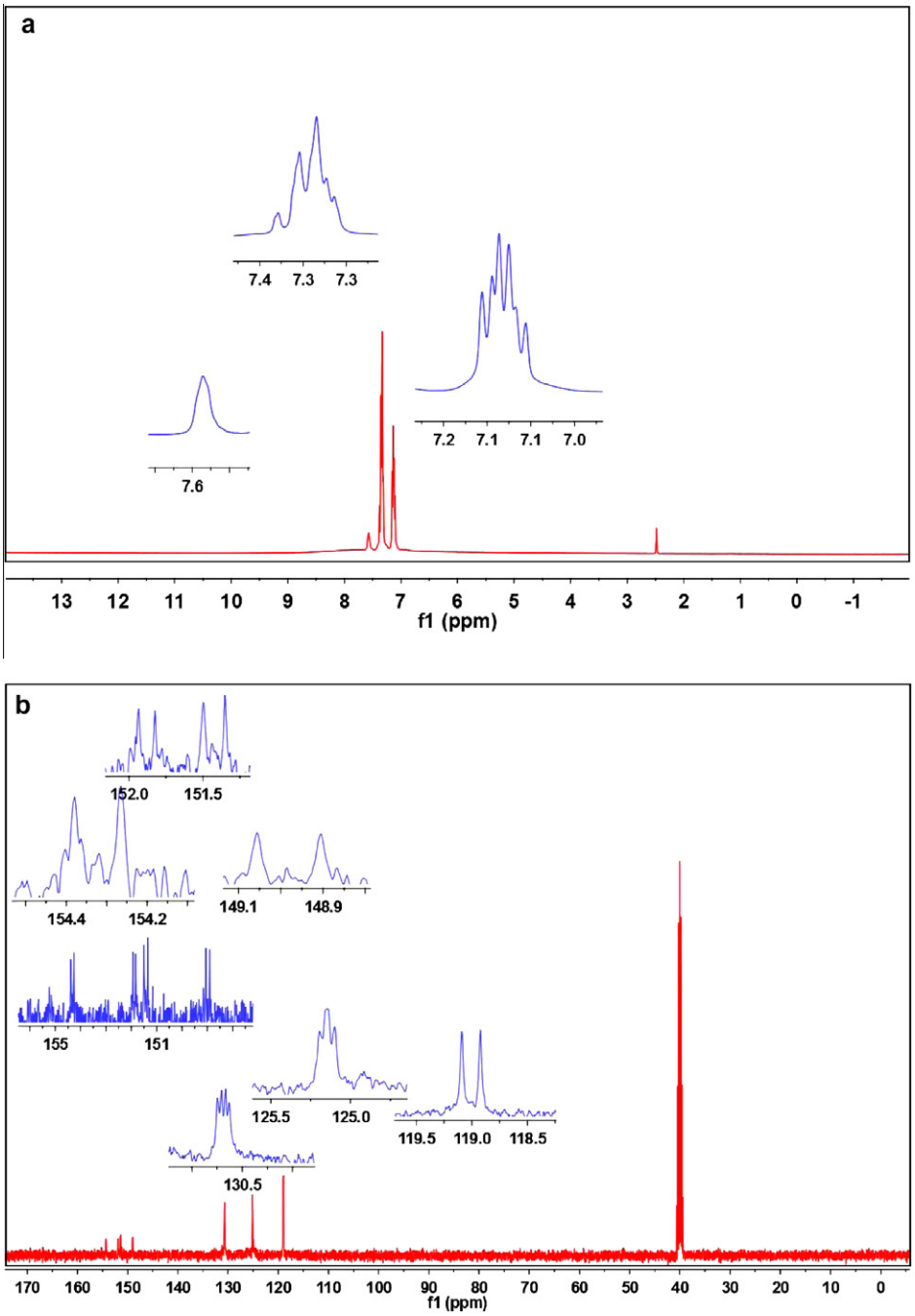


**Fig. 4.** (a) $^{1}$H NMR (b) $^{13}$C NMR spectra of the 2,3-DFPBA in DMSO solution.

**Table 4**
Experimental and theoretical $^{13}$C and $^{1}$H NMR isotropic chemical shifts of the 2,3-DFPBA with DFT (B3LYP 6-311++ G(d,p)) method.

| Atoms | Carbon | | Atoms | Hydrogen | |
|---|---|---|---|---|---|
| | Exp. | B3LYP | | Exp. | B3LYP |
| C(1) | 119.00 | 118.56 | H(10) | 7.15 | 6.88 |
| C(2) | 154.30 | 164.65 | H(11) | 7.11 | 6.02 |
| C(3) | 151.01 | 159.38 | H(12) | 7.38 | 7.44 |
| C(4) | 124.91 | 126.74 | H(13) | 7.31 | 7.32 |
| C(5) | 130.89 | 133.76 | H(14) | 7.57 | 7.94 |
| C(6) | 148.69 | 137.94 | | | |

values are 7.57, 7.38, 7.31, 7.15 and 7.11 ppm. The signals of the three aromatic proton ($^{1}$H) of the title compound were calculated theoretically 7.32–7.94 ppm, observed at 7.31–7.57 ppm experimentally. Chemical shift of proton numbered H14 (observed at 7.57 ppm and calculated at 7.94 ppm) are higher than the other protons. The chemical shift values of H10 and H11 attached the oxygen atoms are smaller than the aromatic proton signals due to the electron withdrawing properties of attached groups. The deviation between experimental and computed chemical shifts of these protons may be due to the presence of intermolecular hydrogen bonding.

The correlation graphics between the experimental and calculated $^{13}$C NMR and $^{1}$H NMR chemical shifts of title molecule are represented in Fig. 5 and Supplementary Fig. S2. The relations between the calculated and experimental wavenumbers chemical shifts ($\delta_{exp}$) and magnetic isotropic shielding tensors ($\sigma$) are usually linear and described by the following equation:

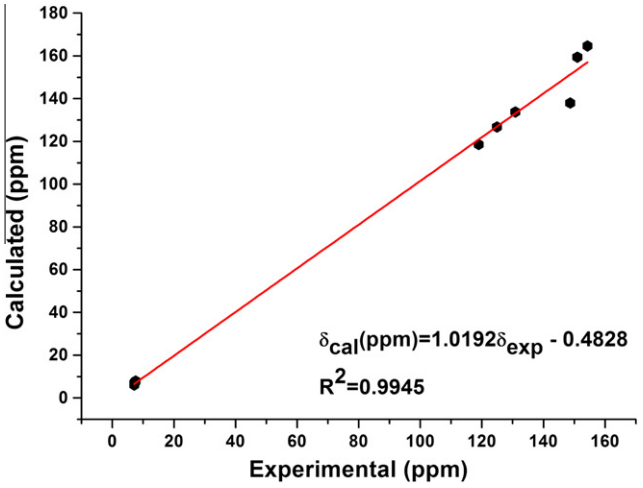


**Fig. 5.** Correlation graphic of calculated and experimental chemical shifts of the 2,3-DFPBA.

$$\delta_{\text{cal.}}(\text{ppm}) = 1.0192\ \delta_{\text{exp.}} - 0.4828 \quad (R^2 = 0.9945)$$

In the present study, the following linear relationships were obtained for $^{13}C$ and $^{1}H$ chemical shifts.

$$\text{For}\ ^{13}\text{C};\ \delta_{\text{cal.}}(\text{ppm}) = 1.1105\ \delta_{\text{exp.}} - 13.221 \quad (R^2 = 0.8401)$$
$$\text{For}\ ^{1}\text{H};\ \delta_{\text{cal.}}(\text{ppm}) = 3.5818\ \delta_{\text{exp.}} - 19.041 \quad (R^2 = 0.8497)$$

The performances of the B3LYP method with respect to the prediction of the relative shielding within the molecule were nearly close. However, $^{1}H$ chemical shifts calculations gave a slightly better coefficient and lower standard error than for $^{13}C$ chemical shifts. Based on the $^{1}H$ and $^{13}C$ chemical shift data collected in Table 4 one can deduce that qualitatively the $^{13}C$ and $^{1}H$ NMR chemical shifts of the 2,3-DFPBA are described fairly well by the selected DFT method combined with the basis set.

## *Electronic properties*

### *UV spectrum and frontier molecular orbital analysis*

Ultraviolet spectra analyses of the 2,3-DFPBA were researched by theoretical calculation and the experiment. The electronic absorption spectra of title molecule were measured in ethanol and water at room temperature. It is obvious that to use TD-DFT calculations to predict the electronic absorption spectra is a quite reasonable method. The excitation energies, absorbance and oscillator strengths for the title molecule at the optimized geometry were obtained in the framework of TD-DFT calculations by using the B3LYP/6-311++G(d,p) method. The experimental absorption wavelengths (energies) and computed electronic values, such as absorption wavelengths ($\lambda$), excitation energies ($E$), oscillator strengths ($f$), and major contributions of the transitions and assignments of electronic transitions are tabulated in Table 5 for ethanol and water solvent. TD-DFT methods are computationally more expensive than semi-empirical methods but they allow to study easily on medium size molecules [69–71]. The experimental and theoretical UV spectra of the 2,3-DFPBA are shown in Fig. 6 for ethanol and water solution. Experimentally determined maximum absorption values in ethanol are 192.0, 208.0 and 266.5 nm, and theoretically calculated values are 251.44, 219.24 and 198.09 nm with B3LYP/6-311++G(d,p) basis set, respectively. For water solution, experimentally determined maximum absorption values are 267.5, 208.5 and 194.0, and theoretically calculated values are 251.40, 219.16 and 198.20 nm, respectively.

Molecular orbitals; both the highest occupied molecular orbital (HOMO) and the lowest unoccupied molecular orbital (LUMO) and their properties such as energy are very useful for physicists and chemists are the main orbital taking part in chemical reaction. While the energy of the HOMO is directly related to the ionization potential, LUMO energy is directly related to the electron affinity [72,73]. This is also used by the frontier electron density for predicting the most reactive position in π-electron systems and also explains several types of reaction in conjugated system [74]. The conjugated molecules are characterized by a small highest occupied molecular orbital–lowest unoccupied molecular orbital (HOMO–LUMO) separation, which is the result of a significant degree of intramolecular charge transfer from the end-capping electron-donor groups to the efficient electron-acceptor group through-π-conjugated path [75]. Surfaces for the frontier orbitals were drawn to understand the bonding scheme of present compound. The energy difference between HOMO and LUMO orbital which is called as energy gap is a critical parameter in determining molecular electrical transport properties because it is a measure of electron conductivity, calculated 5.72 eV for title molecule. The plots of MOs (HOMO and LUMO) are drawn and given in Fig. 7. All the HOMO and LUMO have nodes. The nodes in each HOMO and LUMO are placed symmetrically. The positive phase is red and the negative one is green. According to Fig. 7, the HOMO a charge density localized over the ring of the entire molecule expect $B(OH)_2$ group, but the LUMO is characterized by a charge distribution on all structure, expect H atoms ($H_{10}$ $H_{11}$ and $H_{13}$). The observed transition from HOMO to LUMO is $\pi-\pi^*$. Moreover lower in the HOMO and LUMO energy gap explains the eventual charge transfer interactions taking place within the molecule.

$$\text{HOMO}_{\text{energy}} = -7.40eV$$
$$\text{LUMO}_{\text{energy}} = -1.70eV$$
$$\text{HOMO} - \text{LUMO}_{\text{energy gap}} = 5.70eV$$

The value of chemical hardness is 2.85 eV in gas phase and solvents. However, the values of electronegativity, chemical potential and electrophilicity index are different in gas phase and solvents. These values are given in Table 6.

**Table 5**
Experimental and calculated (TD-DFT/B3LYP/6-311++G(d,p)) absorption wavelengths $\lambda$ (nm), excitation energies (eV), oscillator strengths ($f$) in water and ethanol.

| $\lambda$ (nm) | $E$ (eV) | $\lambda$ (nm) | $E$ (eV) | $f$ | Assignments | Major contributes |
|---|---|---|---|---|---|---|
| *Experimental (Water) Calculated* | | | | | | |
| 267.5 | 4.6349 | 251.40 | 4.9317 | 0.0380 | $\pi-\pi^*$ | H → L (81%), H-1 → L + 1 (18%) |
| 208.5 | 5.9465 | 219.16 | 5.6572 | 0.1456 | $\pi-\pi^*$ | H-1 → L (80%), H → L + 1 (18%) |
| 194.0 | 6.3909 | 198.20 | 6.2556 | 0.0012 | $\pi-\pi^*$ | H → L + 2 (72%), H → L + 3 (26%) |
| *Experimental (Ethanol) Calculated* | | | | | | |
| 266.5 | 4.6523 | 251.44 | 4.9309 | 0.0388 | $\pi-\pi^*$ | H → L (81%), H-1 → L + 1 (18%) |
| 208.0 | 5.9608 | 219.24 | 5.6553 | 0.1488 | $\pi-\pi^*$ | H-1 → L (80%), H → L + 1 (18%) |
| 192.0 | 6.4575 | 198.09 | 6.2591 | 0.0012 | $\pi-\pi^*$ | H → L + 2 (71%), H → L + 3 (27%) |

H: HOMO, L: LUMO.

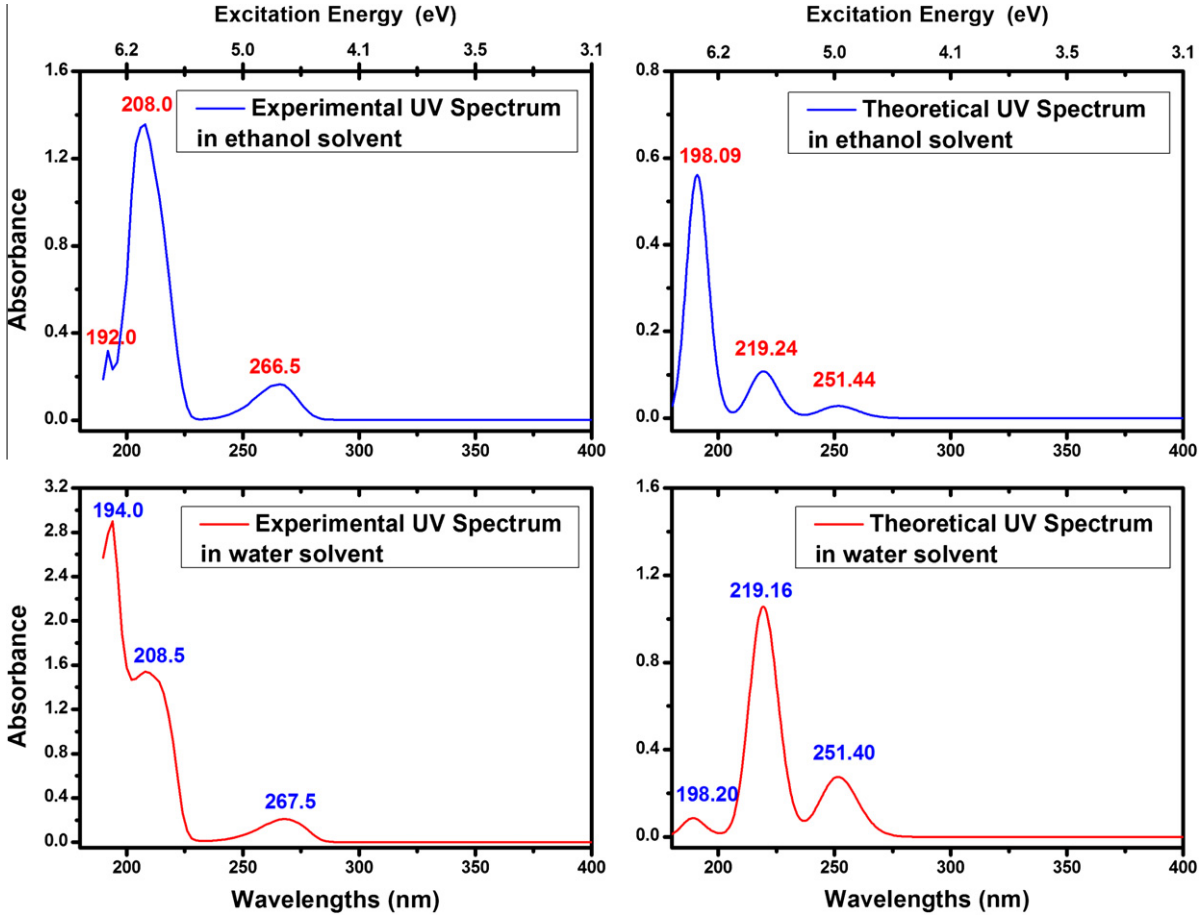


**Fig. 6.** The experimental and theoretical UV–Vis spectrum of the 2,3-DFPBA in ethanol and water.

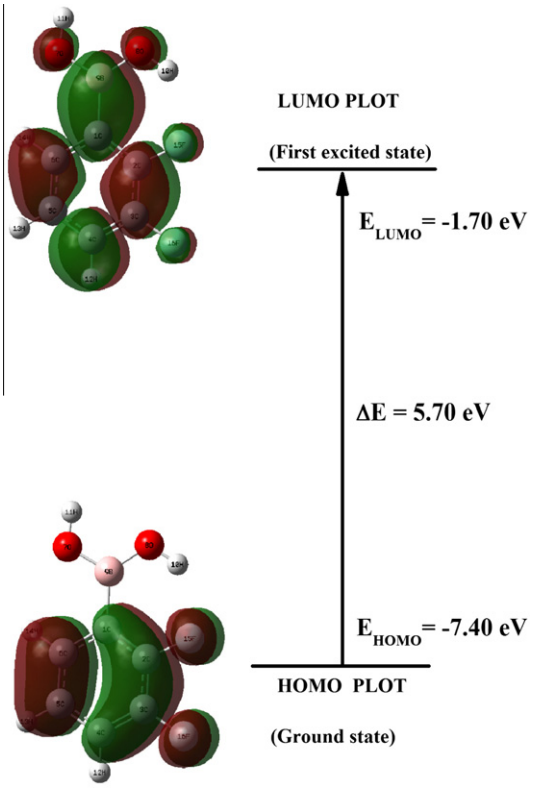


**Fig. 7.** The frontier molecular orbitals of the 2,3-DFPBA for TC conformer.

**Table 6**
Calculated energies values of 2,3-DFPBA molecule using by the TD-DFT/B3LYP method using 6-311++G(d,p) basis set for TC conformer.

| TD-DFT/B3LYP/ 6-311++G(d,p) | Gas | Ethanol | Water |
|---|---|---|---|
| $E_{total}$ (Hartree) | −606.9052395 | −606.9129114 | −606.9132649 |
| $E_{HOMO}$ (eV) | −7.50 | −7.40 | −7.40 |
| $E_{LUMO}$ (eV) | −1.80 | −1.70 | −1.70 |
| $E_{HOMO-LUMO\ gap}$ (eV) | 5.70 | 5.70 | 5.70 |
| $E_{HOMO-1}$ (eV) | −7.90 | −7.78 | −7.78 |
| $E_{LUMO+1}$ (eV) | −1.02 | −0.89 | −0.89 |
| $E_{HOMO-1-LUMO+1\ gap}$ (eV) | 6.88 | 6.89 | 6.89 |
| Chemical hardness (h) | 2.85 | 2.85 | 2.85 |
| Electronegativity (χ) | 4.65 | 4.55 | 4.55 |
| Chemical potential (μ) | −4.65 | −4.55 | −4.55 |
| Electrophilicity index (ω) | 3.79 | 3.63 | 3.63 |

*Total, partial, and overlap population density-of-states*

In the boundary region, neighboring orbitals may show quasi degenerate energy levels. In such cases, consideration of only the HOMO and LUMO may not yield a realistic description of the frontier orbitals. For this reason, the total (TDOS), partial (PDOS), and overlap population (OPDOS or COOP (Crystal Orbital Overlap Population)) density of states [76–78], in terms of Mulliken population analysis were calculated and created by convoluting the molecular orbital information with Gaussian curves of unit height and full width at half maximum (FWHM) of 0.3 eV by using the GaussSum 2.2 program [44]. The TDOS, PDOS and OPDOS of the 2,3-DFPBA are plotted in Figs. 8–10, respectively. They provide a pictorial representation of MO (molecule orbital) compositions

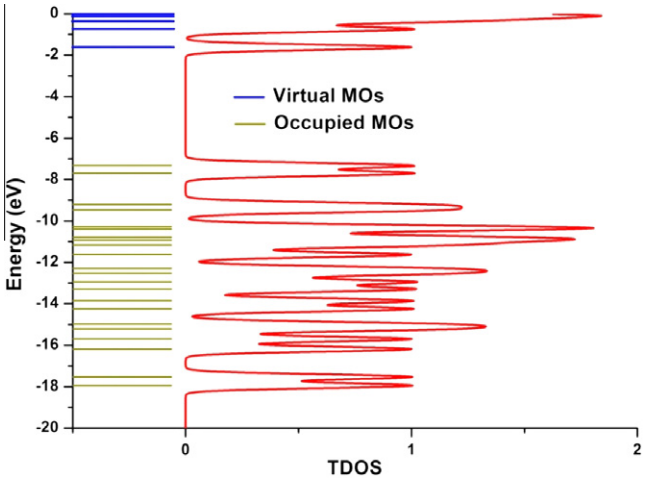


**Fig. 8.** The calculated TDOS diagrams for the 2,3-DFPBA.

and their contributions to chemical bonding. The most important application of the DOS plots is to demonstrate MO compositions and their contributions to the chemical bonding through the OPDOS plots which are also referred in the literature as COOP diagrams. The OPDOS shows the bonding, anti-bonding and nonbonding nature of the interaction of the two orbitals, atoms or groups. A positive value of the OPDOS indicates a bonding interaction (because of the positive overlap population), negative value means that there is an anti-bonding interaction (due to negative overlap population) and zero value indicates nonbonding interactions [79]. Additionally, the OPDOS diagrams allow us to the determine and compare of the donor–acceptor properties of the ligands and ascertain the bonding, non-bonding.

The calculated total electronic density of states (TDOS) diagrams of the 2,3-DFPBA are given in Fig. 8. The partial density of state plot (PDOS) mainly presents the composition of the fragment orbitals contributing to the molecular orbitals which is seen from Fig. 9. As seen Fig. 7, HOMO orbitals are localized on the ring and their contributions are about 100%. The LUMO orbitals are localized on the ring (89%) and $B(OH)_2$ group (11%) of the compound. Only based on the percentage shares of atomic orbitals or molecular fragments in the molecule is difficult to compare groups in terms of its bonding and anti-bonding properties. Thus the OPDOS diagram is shown Fig. 10 and some of orbitals of energy values of interaction between selected groups which are shown from figures easily, $B(OH)_2$ group ↔ fluorine atoms (blue line) system is negative (anti-bonding interaction) as well as 2,3-diflourophenyl ↔ boric acid rings systems (red line). As can be seen from the OPDOS plots for the 2,3-DFPBA have anti-bonding character in frontier HOMO and LUMO molecular orbitals for boronic acid and fluorine atoms. Also OPDOS showed bonding character both HOMO and LUMO.

*Molecular electrostatic potential surface*

The molecular electrostatic potential surface (MEPs) for 2,3-DFPBA molecule in 3D plots is illustrated in Fig. 11. The MEPs is a plot of electrostatic potential mapped onto the constant electron density surface. The MEPs superimposed on top of the total energy density as a shell. Because of the usefulness feature to study reactivity given that an approaching electrophile will be attracted to negative regions (where the electron distribution effect is dominant). In the majority of the MEPs, while the maximum negative region which preferred site for electrophilic attack indications as red color, the maximum positive region which preferred site for nucleophilic attack symptoms as blue color. The importance of MEPs lies in the fact that it simultaneously displays molecular size, shape as well as positive, negative and neutral electrostatic potential regions in terms of color grading and is very useful in research of molecular structure with its physicochemical property relationship [80,81].

The different values of the electrostatic potential at the surface are exemplified by different colors in the map of MEPs. The potential increases in the order from red to blue color. The color code of the maps is in the range between −0.08623 (dark red) and 0.08623 a.u. (dark blue) in compound, where blue indicates the strongest attraction and red indicates the strongest repulsion. As can be seen from the MEPs map of the title molecule, while regions having the positive potential are near OH groups, the regions having the negative potential are over the oxygen atom ($O_7$). From these results, we can say that the $H_{10}$ and $H_{11}$ and fluorine atoms indicate the strongest attraction and $O_7$ atom indicates the strongest repulsion (Fig. 11).

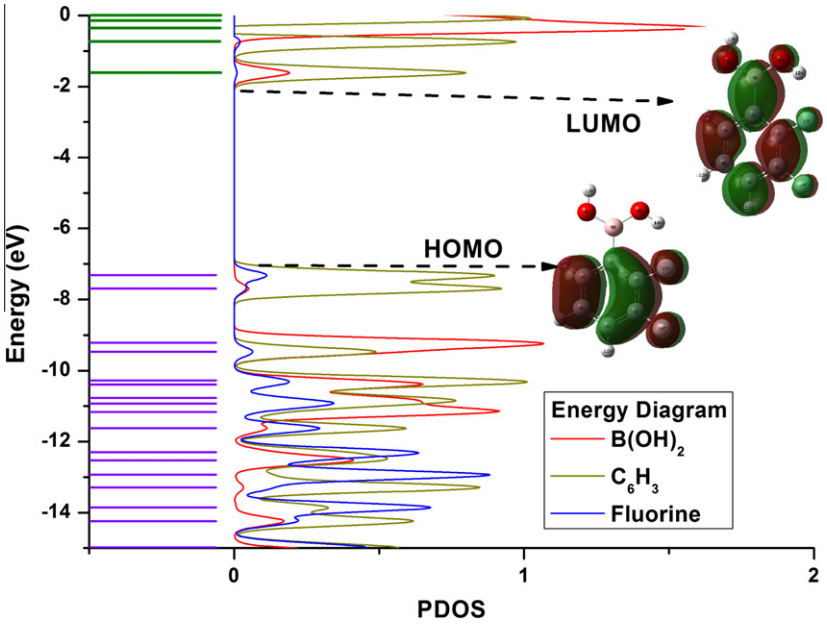


**Fig. 9.** The calculated PDOS diagrams for the 2,3-DFPBA.

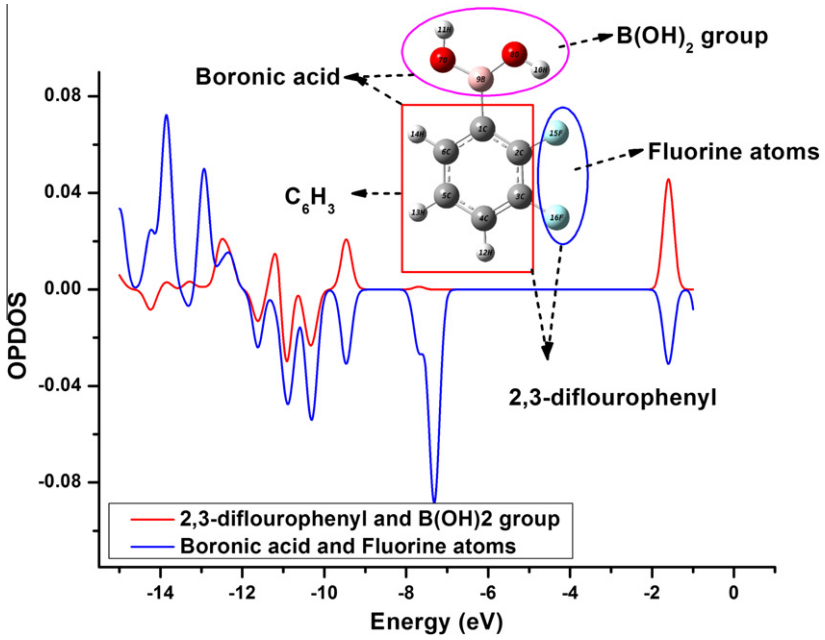


**Fig. 10.** The OPDOS (or COOP) diagrams for the 2,3-DFPBA.

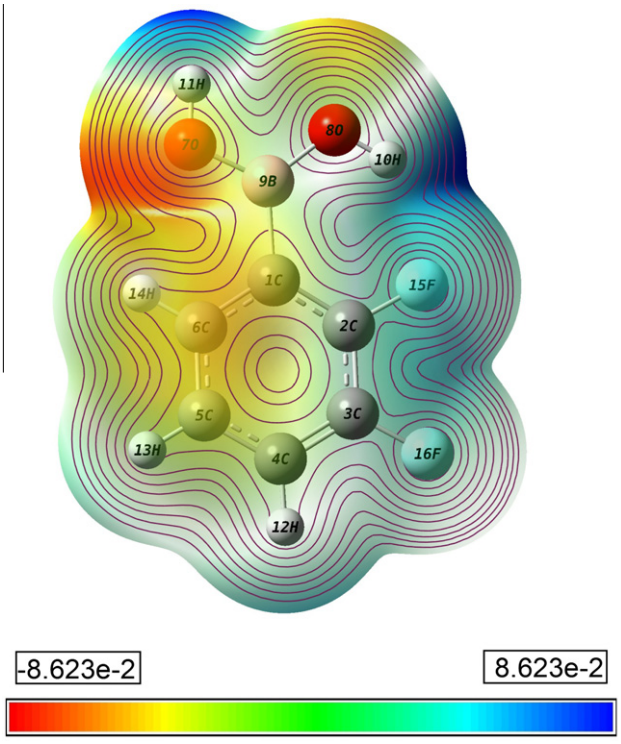


**Fig. 11.** Molecular electrostatic potential map of 2,3-DFPBA.

**Table 7**
Mulliken charges of 2,3-DFPBA and phenylboronic acid using B3LYP/6-311++G(d,p) basis set.

| Atoms | 2,3-DFPBA | Phenylboronic acid |
|---|---|---|
| C1 | 0.080 | −0.680 |
| C2 | −0.193 | 0.206 |
| C3 | −0.257 | −0.352 |
| C4 | 0.343 | −0.022 |
| C5 | −0.364 | −0.439 |
| C6 | −0.171 | 0.188 |
| O7 | −0.393 | −0.377 |
| O8 | −0.378 | −0.366 |
| B9 | 0.590 | 0.531 |
| H10 | 0.251 | 0.230 |
| H11 | 0.293 | 0.288 |
| H12 | 0.209 | 0.161 |
| H13 | 0.177 | 0.161 |
| H14 | 0.200 | 0.196 |
| F15/H15 | −0.206 | 0.114 |
| F16/F16 | −0.181 | 0.160 |

## Mulliken atomic charges

The computation of the reactive atomic charges plays an important role in the application of quantum mechanical calculations for the molecular system. The Mulliken atomic charges of the phenylboronic acid and 2,3-DFPBA are shown in Table 7 and Figs. 12 and 13. Mulliken atomic charges are computed by the DFT/B3LYP method with 6-311++G(d,p) basis set. The results show that substitution of the aromatic ring by fluorine atoms leads to a redistribution of electron density. Namely, the charge of $B(OH)_2$ groups are same distribution (negative or positive) in both molecule, however, ring of molecules exhibit a different charge with each other. For example, the charge of C1 and C4 atoms are negative in phenyl boronic acid, however, because of added fluorine atoms, the values of Mulliken atomic charge of show positive charge in 2,3-DFPBA molecule. While C2 and C6 atoms are positive charge in phenyl boronic acid and negative in 2,3-DFPBA molecule. Hydrogen atoms exhibit a positive charge, which is an acceptor atoms for both two molecules. However, the boron atom has more positive charge than the hydrogen atoms because of the substitution of oxygen atoms of the two-hydroxyl groups. Similarly, the carbon atom shows more negative charge by attracting the negative charge from the boron atom.

## Nonlinear optical properties and dipole moment

The energy of an uncharged liner molecule in a weak, homogenous electric field can be written as

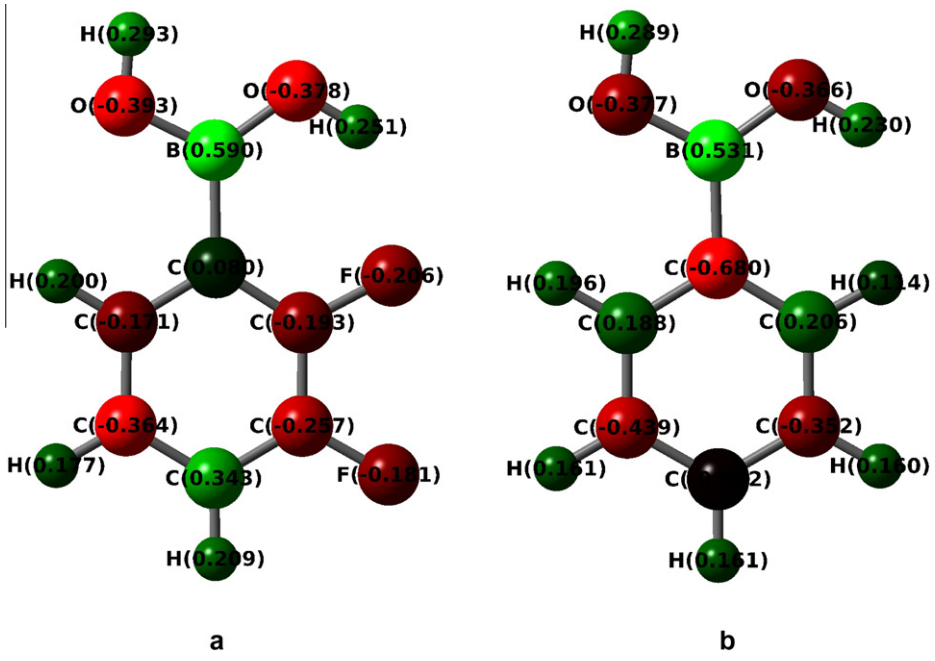


**Fig. 12.** The Mulliken charge distributions for (a) Phenylboronic acid and (b) 2,3-DFPBA.

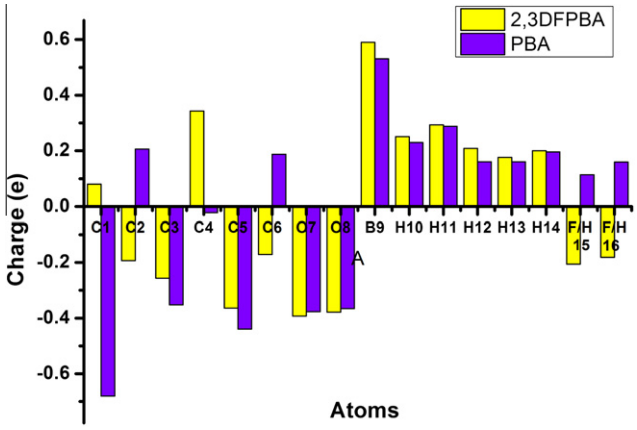


**Fig. 13.** The graphic of calculated Mulliken charge distributions for 2,3-DFPBA.

$$E^p = E^0 - \mu_\alpha F_\alpha - (1/2)\alpha_{\alpha\beta}F_\alpha F_\beta - (1/6)\beta_{\alpha\beta\gamma}F_\alpha F_\beta F_\gamma - (1/24)\gamma_{\alpha\beta\gamma\delta}F_\alpha F_\beta F_\gamma F_\delta + \cdots$$

where $F_{\alpha,\ldots}$ is the filled at the origin and $E^0$ is the energy of the free molecule. The molecular properties are the dipole moment ($\mu_\alpha$), polarizability ($\alpha_{\alpha\beta}$), first ($\beta_{\alpha\beta\gamma}$) hyperpolarizability and second order ($\gamma_{\alpha\beta\gamma}$) hyperpolarizability. The number of independent components for these tensors is regulated by symmetry. In the presence of an applied electric field, the energy of a system is a function of the electric field. First hyperpolarizability is a third rank tensor that can be described by a $3 \times 3 \times 3$ matrix and the 27 components of the 3D matrix can be reduced to 10 components due to the Kleinman symmetry [82].

In this study, the electronic dipole moment, molecular polarizability, anisotropy of polarizability and molecular first hyperpolarizability of present compound were investigated. The polarizability and hyperpolarizability tensors ($\alpha_{xx}$, $\alpha_{xy}$, $\alpha_{yy}$, $\alpha_{xz}$, $\alpha_{yz}$, $\alpha_{zz}$ and $\beta_{xxx}$, $\beta_{xxy}$, $\beta_{xyy}$, $\beta_{yyy}$, $\beta_{xxz}$, $\beta_{xyz}$, $\beta_{yyz}$, $\beta_{xzz}$, $\beta_{yzz}$, $\beta_{zzz}$) can be obtained by a frequency job output file of Gaussian. However, $\alpha$ and $\beta$ values of Gaussian output are in atomic units (a.u.) so they have been converted into electronic units (esu) ($\alpha$; 1 a.u. = $0.1482 \times 10^{-24}$ esu, $\beta$; 1 a.u. = $8.6393 \times 10^{-33}$ esu). The mean polarizability ($\alpha$), anisotropy of polarizability ($\Delta\alpha$) and the average value of the first hyperpolarizability $\langle\beta\rangle$ can be calculated using the equations.

$$\alpha_{tot} = \frac{1}{3}(\alpha_{xx} + \alpha_{yy} + \alpha_{zz})$$

$$\Delta\alpha = \frac{1}{\sqrt{2}}[(\alpha_{xx} - \alpha_{yy})^2 + (\alpha_{yy} - \alpha_{zz})^2 + (\alpha_{zz} - \alpha_{xx})^2 + 6\alpha_{xz}^2 + 6\alpha_{xy}^2 + 6\alpha_{yz}^2]^{\frac{1}{2}}$$

$$\langle\beta\rangle = [(\beta_{xxx} + \beta_{xyy} + \beta_{xzz})^2 + (\beta_{yyy} + \beta_{yzz} + \beta_{yxx})^2 + (\beta_{zzz} + \beta_{zxx} + \beta_{zyy})^2]^{\frac{1}{2}}$$

In Table 8, the calculated parameters described above and electronic dipole moment {$\mu_i$ ($i$ = x, y, z) and total dipole moment $\mu_{tot}$} for title compound are listed. The total dipole moment can be calculated using the following equation.

$$\mu_{tot} = (\mu_x^2 + \mu_y^2 + \mu_z^2)^{\frac{1}{2}}$$

It is well known that the higher values of dipole moment, molecular polarizability, and hyperpolarizability are important for more active NLO properties. 2,3-DFPBA has relatively homogeneous charge dis-

**Table 8**
The dipole moments μ (D), the polarizability α (a.u.), the average polarizability $\alpha_o$ (esu), the anisotropy of the polarizability Δα (esu), and the first hyperpolarizability β (esu) of 2,3-DFPBA.

| | | | |
|---|---|---|---|
| $\mu_x$ | 0.040359 | $\beta_{xxx}$ | 1363.259295 |
| $\mu_y$ | 0.634613 | $\beta_{xxy}$ | 33.337539 |
| $\mu_z$ | 0.0 | $\beta_{xyy}$ | −61.574080 |
| $\mu_0$ | 0.635895 | $\beta_{yyy}$ | 1746.468392 |
| $\alpha_{xx}$ | 16.813043 | $\beta_{xxz}$ | 0.0 |
| $\alpha_{xy}$ | −0.521446 | $\beta_{xyz}$ | 0.0 |
| $\alpha_{yy}$ | 14.652546 | $\beta_{yyz}$ | 0.0 |
| $\alpha_{xz}$ | 0.0 | $\beta_{xzz}$ | −49.715797 |
| $\alpha_{yz}$ | 0.0 | $\beta_{yzz}$ | 551.666616 |
| $\alpha_{zz}$ | 7.516433 | $\beta_{zzz}$ | 0.0 |
| $\alpha_{total}$ | 12.994007 | $\beta_x$ | 1251.969442 |
| Δα | 30.315750 | $\beta_y$ | 2331.472547 |
| | | $\beta_z$ | 0.0 |
| | | β | 2646.354409 |

tribution and it does not have large dipole moment. The calculated value of dipole moment was found to be 0.635895 Debye. The highest value of dipole moment is observed for component $\mu_y$. In this direction, this value is equal to 0.634613 D and $\mu_z$ is zero. The calculated polarizability and anisotropy of the polarizability of 2,3-DFPBA is $12.9940 \times 10^{-24}$ and $30.3157 \times 10^{-24}$ esu, respectively. The magnitude of the molecular hyperpolarizability β, is one of important key factors in a NLO system. The B3LYP/6-311++G(d,p) calculated first hyperpolarizability value (β) of NA is equal to $2646.3544 \times 10^{-33}$ esu. Urea is one of the prototypical molecules used in the study of the NLO properties of molecular systems. Therefore it was used frequently as a threshold value for comparative purposes. The first hyperpolarizability, polarizability and anisotropy of the polarizability values of 2,3-DFPBA are larger than those of urea. The first hyperpolarizability value is ca. 3.5 times larger than urea ones. However, the dipole moment value is ca. two times smaller than those of urea. The β, α, Δα and μ of urea are $780.324 \times 10^{-33}$, $5.0477 \times 10^{-24}$, $9.8688 \times 10^{-24}$ esu, and 1.52569 Debye and obtained by using B3LYP/6-311++G(d,p) method.

## Thermodynamic properties

On the basis of vibrational analysis at B3LYP/6-311++G(d,p) level, the standard statistical thermodynamic functions: heat capacity, entropy and enthalpy changes for the title compound were obtained from the theoretical harmonic frequencies and listed in Table 9. From Table 9, it can be observed that these thermodynamic functions are increasing with temperature ranging from 100 to 700 K due to the fact that the molecular vibrational intensities increase with temperature. The correlation equations between heat capacity, entropy, enthalpy changes and temperatures are fitted by quadratic formulas. The corresponding fitting factors ($R^2$) for these thermodynamic properties are 0.9998, 1.0000 and 0.9997, respectively. The corresponding fitting equations are as follows and the correlation graphics of those shows in Figs. 14–16.

$$C = -0.2134 + 0.1442T - 7.7170 \times 10^{-5}T^2 \quad (R^2 = 0.9998)$$
$$S = 53.2039 + 0.1548T - 5.5368 \times 10^{-5}T^2 \quad (R^2 = 1.0000)$$
$$H = -0.7260 + 0.0123T + 4.1498 \times 10^{-5}T^2 \quad (R^2 = 1.0000)$$

All the thermodynamic data supply helpful information for the further study on the 2,3-DFPBA. They can be used to compute the other thermodynamic energies according to relationships of thermodynamic functions and estimate directions of chemical reactions according to the second law of thermodynamics in thermochemical field. Notice: all thermodynamic calculations were done in gas phase and they could not be used in solution.

**Table 9**
Thermodynamic properties at different temperatures at the B3LYP/6-311++G(d,p) level of 2,3-DFPBA.

| $T$ (K) | $C$ (cal mol$^{-1}$ K$^{-1}$) | S (cal mol$^{-1}$ K$^{-1}$) | $\Delta H$ (kcal mol$^{-1}$) |
|---|---|---|---|
| 100 | 13.959 | 68.032 | 1.134 |
| 150 | 19.434 | 75.516 | 2.065 |
| 200 | 25.150 | 82.461 | 3.279 |
| 250 | 30.743 | 89.122 | 4.777 |
| 300 | 36.034 | 95.562 | 6.547 |
| 350 | 40.916 | 101.796 | 8.572 |
| 400 | 45.327 | 107.818 | 10.830 |
| 450 | 49.255 | 113.622 | 13.295 |
| 500 | 52.720 | 119.204 | 15.946 |
| 550 | 55.766 | 124.564 | 18.759 |
| 600 | 58.444 | 129.707 | 21.715 |
| 650 | 60.805 | 134.639 | 24.797 |
| 700 | 62.897 | 139.371 | 27.990 |

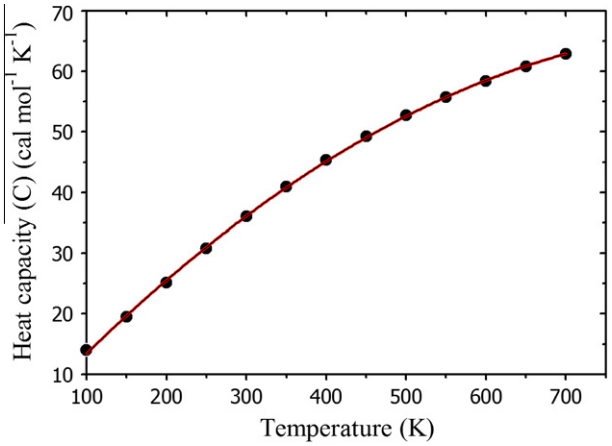


**Fig. 14.** Correlation graphic of heat capacity and temperature for 2,3-DFPBA.

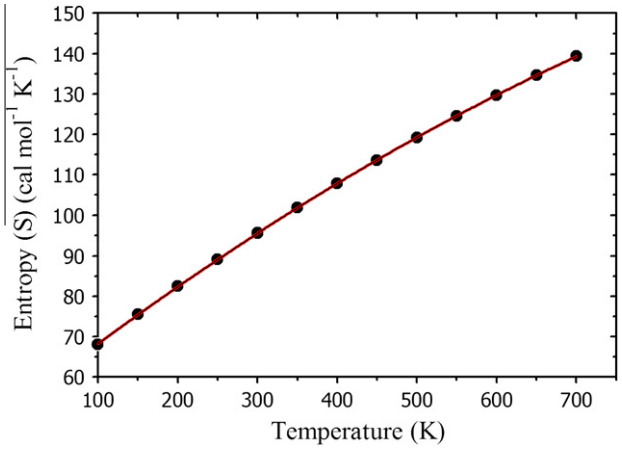


**Fig. 15.** Correlation graphic of entropy and temperature for 2,3-DFPBA.

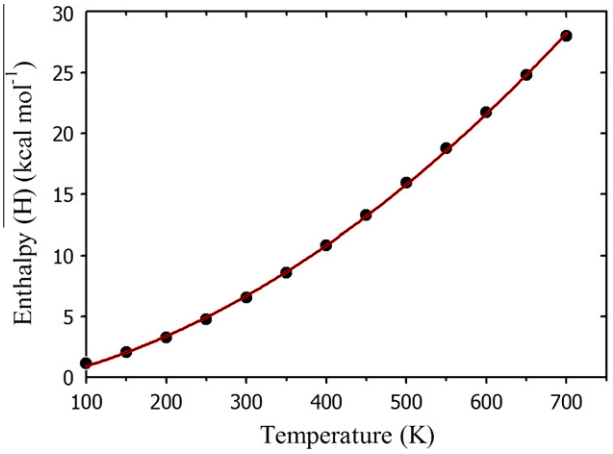


**Fig. 16.** Correlation graphic of enthalpy and temperature for 2,3-DFPBA.

The values of some thermodynamic parameters (such as zero-point vibrational energy, thermal energy, specific heat capacity, rotational constants, entropy, etc.) of 2,3-DFPBA at 298.15 K in ground state are listed in Table 10. The variation in Zero-Point Vibrational Energies (ZPVEs) seems to be significant. The biggest values of ZPVE of 2,3-DFPBA (TC conformer is most stable struc-

**Table 10**
The calculated thermo dynamical parameters of 2,3-DFPBA at 298.15 K in ground state at the B3LYP/6-311++G(d,p) level.

| Conformers | *Trans–cis (TC)* | *Cis–cis (CC)* | *Cis–trans (CT)* | *Trans–trans (TT)* |
|---|---|---|---|---|
| *Cs symmetry* | | | | |
| SCF energy (a.u.) | −606.93076996 | −606.92307536 | −606.92239190 | −606.92070450 |
| Zero point vib. energy (kcal $mol^{-1}$) | −68.27287 | −67.81956 | −67.76079 | −67.74402 |
| Rotational constants (GHz) | 1.87357 | 1.8697 | 1.88039 | 1.87259 |
| | 0.85443 | 0.85303 | 0.84868 | 0.85462 |
| | 0.58682 | 0.58577 | 0.58476 | 0.58681 |
| Specific heat, *Cv* (cal $mol^{-1}$ $K^{-1}$) | 35.845 | 34.437 | 34.381 | 36.484 |
| Entropy, *S* (cal $mol^{-1}$ $K^{-1}$) | 95.328 | 91.377 | 91.554 | 97.757 |
| *C1 symmetry* | | | | |
| SCF energy (a.u.) | −606.93074912 | −606.92316278 | −606.92323320 | −606.92067554 |
| Zero point vib. energy (kcal $mol^{-1}$) | −68.27064 | −68.10032 | −67.99223 | −67.71813 |
| Rotational constants (GHz) | 1.87324 | 1.86773 | 1.87037 | 1.87261 |
| | 0.85476 | 0.85198 | 0.83530 | 0.85440 |
| | 0.58694 | 0.58779 | 0.59689 | 0.58671 |
| Specific heat, *Cv* (cal $mol^{-1}$ $K^{-1}$) | 35.840 | 36.080 | 36.069 | 36.519 |
| Entropy, *S* (cal $mol^{-1}$ $K^{-1}$) | 95.344 | 96.536 | 97.027 | 97.922 |

ture) are −68.27287 and −68.27064 kcal/mol for Cs and C1 symmetry group.

## Conclusions

The investigation of the present work is illuminate the spectroscopic properties such as molecular parameters, frequency assignments, electronic transition and magnetic properties of title compound by using FT-IR, FT-Raman UV–Vis, $^{1}H$ and $^{13}C$ NMR techniques and tools derived from the density functional theory. A conformational analysis was carried out by means of molecular dynamics simulations. The most stable conformer identified as *TC*. Due to the lack of experimental information on the structural parameters available in the literature, the optimized geometric parameters (bond lengths and bond angles) was theoretically determined at B3LYP/6-311++G(d,p) level of theory and compared with the structurally similar compounds. The vibrational FT-IR and FT-Raman spectra of the 2,3-DFPBA were recorded and computed vibrational wavenumbers and their TED were calculated. The magnetic properties of the title molecule were observed and calculated the same method. The chemical shifts were compared with experimental data in DMSO solution, showing a very good agreement both for $^{13}C$ and $^{1}H$ chemical shifts. The electronic properties were also calculated and the experimental electronic spectrum was recorded with help of UV–Vis spectrometer. When all theoretical results scanned, they are showing good correlation with experimental data.

## Acknowledgement

This work was supported by the Celal Bayar University Research fund through research Grant no. FBE-2011/70.

## Appendix A. Supplementary data

Supplementary data associated with this article can be found, in the online version, at http://dx.doi.org/10.1016/j.saa.2012.07.077.

## References

[1] A.H. Soloway, R.G. Fairchild, Sci. Am. 262 (1990) 100.
[2] D.A. Matthews, R.A. Alden, J.J. Birktoft, S.T. Freer, J. Kraut, J. Biol. Chem. 250 (1975) 7120.
[3] D.H. Kinder, S.K. Frank, M.M. Ames, J. Med. Chem. 33 (1990) 819–823.
[4] X. Chen, G. Liang, D. Whitmire, J.P. Bowen, J. Phys.Org. Chem. 11 (1988) 378.
[5] W. Tjarks, A.K.M. Anisuzzaman, L. Liu, S.H. Soloway, R.F. Barth, D.J. Perkins, D.M. Adams, J. Med. Chem. 35 (1992) 16228–17861.
[6] Y. Yamamoto, Pure Appl. Chem. 63 (1991) 423.
[7] F. Alam, A.H. Soloway, R.F. Barth, N. Mafune, D.M. Adam, W.H. Knoth, J. Med. Chem. 32 (1989) 2326–2330.
[8] M.R. Stabile et al., Bioorg. Med. Chem. Lett. 21 (1996) 2501–2506.
[9] P.R. Westmark, B.D. Smith, J. Pharm. Sci. 85 (1996) 266–269.
[10] M.K. Cyrański, A. Jezierska, P. Klimentowska, J.J. Panek, A. Sporzyński, J. Phys. Org. Chem. 21 (2008) 472–482.
[11] S.J. Rettig, J. Trotte, Can. J. Chem. 55 (1977) 3071–3075.
[12] P.N. Horton, M.B. Hursthouse, M.A. Becket, M.P.R. Hankey, Acta Cryst. E60 (2004) o2204–o2206.
[13] M.R. Shimpi, N.S. Lekshmi, V.R. Pedireddi, Cryst. Growth Des. 7 (10) (2007) 1958–1963.
[14] Y-M. Wu, C-C. Dong, S. Liu, H-J. Zhu, Y-Z. Wu, Acta Cryst. E62 (2006) o4236–o4237.
[15] D.C. Bradley, I.S. Harding, A.D. Keefe, M. Motevalli, D.H. Zheng, J. Chem. Soc. Dalton Trans. (1996) 3931–3936.
[16] P.R. Cuamatzi, H. Tlahuext, H. Höpfl, Acta Cryst. E65 (2009) o44–o45.
[17] A. Vega, M. Zarate, H. Tlahuext, H. Hopfl, Acta Cryst. E66 (2010) o1260–o1261.
[18] B. Zarychta, J. Zaleski, A. Sporzynski, M. Dabrowski, J. Serwatowski, Acta Cryst. C60 (2004) o344–o345.
[19] J.A. Faniran, H.F. Shurvell, Can. J. Chem. 46 (1968) 2089–2095.
[20] Y. Erdogdu, M.T. Gulluoglu, M. Kurt, J. Raman Spectrosc. 40 (2009) 1615–1623.
[21] M. Kurt, J. Mol. Struct. 874 (2008) 159–169.
[22] S. Ayyappan, N. Sundaraganesan, M. Kurt, T.R. Sertbakan, M. Ozduran, J. Raman Spectrosc. 41 (2010) 1379–1387.
[23] M. Kurt, T.R. Sertbakan, M. Ozduran, M. Karabacak, J. Mol. Struct. 921 (2009) 178–187.
[24] M. Kurt, J. Raman Spectrosc. 40 (2009) 67–75.
[25] O. Alver, C.R. Chimie 14 (2011) 446–455.
[26] O. Alver, C. Parlak, Vib. Spectr. 54 (2010) 1–9.
[27] K.L. Bhat, N.J. Howard, H. Rostami, J.H. Lai, Charles W. Bock, J. Mol. Struct. (Theochem) 723 (2005) 147–157.
[28] M. Kurt, T.R. Sertbakan, M. Özduran, Spectrochim. Acta 70 (2008) 664–673.
[29] M.K. Cyrański, A. Jezierska, P. Klimentowska, J.J. Panek, A. Sporzyński, J. Chem. Phys. 128 (2008) 124512.
[30] U. Rani, M. Karabacak, O. Tanrıverdi, M. Kurt, N. Sundaraganesan, Spectrochim. Acta 92 (2012) 67–77.
[31] N.C. Handy, C.W. Murray, R.D. Amos, J. Phys. Chem. 97 (1993) 4392.
[32] P.J. Stephens, F.J. Devlin, C.F. Chabalowski, M.J. Frisch, J. Phys. Chem. 98 (1994) 11623–11627.
[33] F.J. Devlin, J.W. Finley, P.J. Stephens, M.J. Frish, J. Phys. Chem. 99 (1995) 16883–16902.
[34] S.Y. Lee, B.H. Boo, Bull. Korean Chem. Soc. 17 (1996) 760–764.
[35] G. Rauhut, P. Pulay, J. Phys. Chem. 99 (1995) 3093.
[36] P. Hohenberg, W. Kohn, Phys. Rev. 136 (1964) B864–B871.
[37] A.D. Becke, J. Chem. Phys. 98 (1993) 5648–5652.
[38] C. Lee, W. Yang, R.G. Parr, Phys. Rev. 37 (1988) 785–789.
[39] M.J. Frisch et al., Gaussian, Inc., Wallingford, CT, 2009.
[40] N. Sundaraganesan, S. Ilakiamani, H. Salem, P.M. Wojciechowski, D. Michalska, Spectrochim. Acta 61 (2005) 2995–3001.
[41] J. Baker, A.A. Jarzecki, P. Pulay, J. Phys. Chem. A102 (1998) 1412–1424.
[42] P. Pulay, J. Baker, K. Wolinski, 2013 Green Acres Road, Suite A, Fayettevile, USA, AR72703.
[43] K. Wolinski, J.F. Hinton, P. Pulay, J. Am. Chem. Soc. 112 (1990) 8251–8260.
[44] N.M. O'Boyle, A.L. Tenderholt, K.M. Langner, J. Comp. Chem. 29 (2008) 839–845.
[45] N. Sundaraganesan, B. Anand, C. Meganathan, B.D. Joshua, Spectroch. Acta 68 (2007) 561–566.
[46] C. Par, E.T. Bavoux, P. Michel, Acta Cryst. 30 (1974) 2043–2045.
[47] A.R. Choudhury, T.N. Guru Row, Acta Cryst. E60 (2004) o1595–1597.
[48] M. Karabacak, E. Kose, M. Kurt, J. Raman Spectrosc. 41 (2010) 1085–1097.
[49] L.J. Bellamy, The Infrared Spectra of Complex Molecules, Wiley, New York, 1959.

[50] M. Silverstein, G. Clayton Basseler, C. Morill, Spectrometric Identification of Organic Compounds, Wiley, New York, 2001.
[51] V. Arjunan, I. Saravanan, P. Ravindran, S. Mohan, Spectrochim. Acta 74 (2009) 375–384.
[52] G. Varsanyi, Assignments of Vibrational Spectra of Seven Hundred Benzene Derivatives, Adam Hilger 1-2 (1974).
[53] C.N.R. Rao, Chemical Applications of Infrared Spectroscopy, Academic Press, New York, 1959.
[54] N.A. Narasimham, M.Z. El-Saban, J. Rud-Nielson, J. Chem. Phys. (USA) 24 (1956) 420.
[55] E.E. Ferguson et al., J. Chem. Phys. (USA) 21 (1953) 1464.
[56] A.K. Ansari, P.K. Verma, Spectrochim. Acta 35 (1979) 35.
[57] A. Papagni, S. Mairona, P.D. Buttero, D. Perdiccia, F. Cariati, E. Cariati, W. Marcolli, Eur. J. Org. Chem. (2002) 1380–1384.
[58] K. Koppe, PhD. Thesis, Duisburg University, 2005.
[59] M.S. Navati, M.A. Shashindhar, Ind. J. Phys. 66B (1994) 371.
[60] N. Sundaraganesan, S. Ilakiamani, B.D. Joshua, Spectrochim. Acta 67 (2007) 287–297.
[61] L. Santuci, H. Gilman, J. Am. Chem. Soc. 80 (1958) 193–196.
[62] S.H. Brewer, A.M. Allen, S.E. Lappi, T.L. Chase, K.A. Briggman, C.B. Gorman, S. Franzen, Langmuir 20 (2004) 5512.
[63] V. Krishnakumar, V. Balachandran, Spectrochim. Acta 61 (2005) 1001–1006.
[64] G. Kahraman, O. Beskarcles, Z.M. Rzave, E. Piskin, Polymer 45 (2004) 5813–5828.
[65] G. Vargas, I. Hernandez, H. Höpfl, M. Ochoa, D. Castillo, N. Farfan, R. Santillan, E. Gomez, Inorg. Chem. 43 (2004) 8490–8500.
[66] H.O. Kalinowski, S. Berger, S. Braun, Carbon-13 NMR spectroscopy, John Wiley & Sons, Chichester, 1988.
[67] K. Pihlaja, E. Kleinpeter (Eds.), Carbon-13 Chemical Shifts in Structural and Sterochemical Analysis, VCH Publishers, Deerfield Beach, 1994.
[68] N. Subramania, N. Sundaraganesan, J. Jayabharathi, Spectrochim. Acta 76 (2010) 259–269.
[69] D. Guillaumont, S. Nakamura, Dyes Pigm. 46 (2000) 85–92.
[70] J. Fabian, Dyes Pigm. 84 (2010) 36–53.
[71] L. Briquet, D.P. Vercauteren, J.M. André, E.A. Perpète, D. Jacquemin, Chem. Phys. Lett. 435 (2007) 257–262.
[72] K. Fukui, Science 218 (1982) 747–754.
[73] S. Gunasekaran, R.A. Balaji, S. Kumeresan, G. Anand, S. Srinivasan, Can. J. Anal. Sci. Spectrosc. 53 (2008) 149–162.
[74] K. Fukui, T. Yonezawa, H. Shingu, J. Chem. Phys. 20 (1952) 722–725.
[75] C.H. Choi, M. Kertesz, J. Phys. Chem. 101A (1997) 3823–3831.
[76] R. Hoffmann, Solids and Surfaces: A Chemist's View of Bonding in Extended Structures, VCH Publishers., New York, 1988.
[77] T. Hughbanks, R. Hoffmann, J. Am. Chem. Soc. 105 (1983) 3528–3537.
[78] J.G. Małecki, Polyhedron 29 (2010) 1973–1979.
[79] M. Chen, U.V. Waghmare, C.M. Friend, E. Kaxiras, J. Chem. Phys. 109 (1998) 6680–6854.
[80] J.S. Murray, K. Sen, Molecular electrostatic potentials, Concepts and Applications, Elsevier, Amsterdam, 1996.
[81] E. Scrocco, J. Tomasi, in: P. Lowdin (Ed.), Advances in Quantum Chemistry, Academic Press, New York, 1978.
[82] D.A. Kleinman, Phys. Rev. 126 (1962) 1977–1979.